

A high spatial resolution X-ray and H α study of hot gas in the halos of star-forming disk galaxies. II. Quantifying supernova feedback

David K. Strickland,^{1,2} Timothy M. Heckman,² Edward J.M. Colbert,² Charles G. Hoopes,² and Kimberly A. Weaver.³

ABSTRACT

We investigate how the empirical properties of hot X-ray-emitting gas in a sample of seven starburst and 3 normal edge-on spiral galaxies (a sample which covers the full range of star-formation intensity found in disk galaxies) correlate with the size, mass, star formation rate and star formation intensity in the host galaxies. From this analysis we investigate various aspects of mechanical energy “feedback”—the return of energy to the ISM from massive star supernovae and stellar winds—on galactic scales. The X-ray observations make use of the unprecedented spatial resolution of the *Chandra* X-ray observatory to robustly remove X-ray emission from point sources, and hence obtain the X-ray properties of the diffuse thermal emission alone. We demonstrate, using a variety of multi-wavelength star formation rate and intensity indicators, that the diffuse X-ray emission is ultimately driven by mechanical energy feedback from massive stars. We find that the luminosity of the extra-planar diffuse X-ray emission is proportional to proxies of the star formation rate of the host galaxy, for example the FIR or 1.4 GHz radio luminosity. Larger galaxies tend to have more extended X-ray-emitting halos, but galaxy mass appears to play no role in determining the properties of the disk or extra-planar X-ray emitting plasma. Accretion of gas from the IGM does not appear to be a significant contributor to the diffuse X-ray emission in this sample. The combination of these luminosity and size correlations leads to a correlation between the surface brightness of the diffuse X-ray emission and the mean star formation rate per unit area in the disk L_{FIR}/D_{25}^2 . Intriguingly, the diffuse X-ray properties of the normal spirals (both in their disks and halos) fall where extrapolation of the trends from the starburst galaxies with superwinds would predict. We reconsider the conditions necessary for superbubble blow-out from the disk into the halo of a galaxy, and present methods for observationally determining the efficiency of mechanical energy feedback and testing theoretical models of disk blow out. We further consider blow out of gas into the IGM from the extended gaseous halos around star-forming galaxies. We argue that the crucial spatial region around a galaxy that controls whether gas will escape into the IGM is not the outer halo ~ 100 kpc from the host galaxy, but the inner few halo scale heights, within ~ 20 kpc of the galaxy plane. Given the properties of the gaseous halos we observe, outflows from disk galaxies of mass $M \sim 10^{10} - 10^{11} M_{\odot}$ should still eject some fraction of their material into the IGM.

Subject headings: ISM: jets and outflows — ISM: bubbles — galaxies: individual (NGC 253; NGC 891; NGC 1482; NGC 3034 (M82); NGC 3073; NGC 3079; NGC 3628; NGC 4244; NGC 4631; NGC 4945; NGC 6503) — galaxies: halos — galaxies: starburst — X-rays: galaxies

1. Introduction

¹*Chandra* Fellow.

²Department of Physics and Astronomy, The Johns Hopkins University, 3400 North Charles Street, Baltimore, MD 21218

³NASA/Goddard Space Flight Center, Code 662, Greenbelt, Maryland 20771

Massive stars exercise a profound influence over the baryonic component of the Universe, through the return of ionizing radiation, and via supernovae (SNe), kinetic energy and metal-enriched gas, back into the interstellar medium (ISM) from which they form —

usually called “feedback”. Feedback influences gas-phase conditions in the immediate environment of the clusters within which the massive stars form (McKee 1995; Hollenbach & Tielens 1997; Wiseman & Ho 1998; Pudritz & Fiege 2000), on galactic scales the phase structure and energetics of the ISM (McKee & Ostriker 1977; Cox 1981; Norman & Ikeuchi 1989; Norman & Ferrara 1996), and on multi-Mpc scales the thermodynamics and enrichment of the inter-galactic medium (IGM — e.g. see Chiang, Ryu & Vishniac 1988; Heckman, Armus & Miley 1990; Shapiro, Giroux & Babul 1994; Voit 1996; Heckman 1999; Aguirre et al. 2001).

The vast range of spatial scales involved is only one of the difficulties encountered in attempting to study feedback. Restricting the discussion to purely mechanical feedback from SNe and stellar winds (commonly termed SN feedback), a further difficulty is the broad range of complicated gas-phase physics — (magneto)hydrodynamic effects such as shocks and turbulence, thermal conduction, and non-ionization equilibrium emission processes. A final complication is that much of the energy and metal-enriched material involved is in the hard-to-observe coronal ($T \gtrsim 10^5$ K) and hot ($T \gtrsim 10^6$ K) gas phases, necessitating the use of space-based FUV and X-ray telescopes.

X-ray observations of the halo-regions of nearby edge-on disk galaxies provide the best single probe of the action of mechanical feedback on the galactic scale. Optical spectroscopy and imaging, sensitive to warm neutral and ionized gas with $T \sim 10^4$ K, are a less direct probe of mechanical feedback as much of the excitation energy is supplied by ionizing radiation from massive stars (radiative feedback), even when the kinematics and spatial distribution of this gas are controlled by SN feedback. If mechanical feedback processes transport mass, newly-synthesized metals, and energy from galaxies into the IGM, then this material must pass through the halo of the host galaxy on its way into the IGM, where its properties can be ascertained before it expands and fades into observational invisibility.

Diffuse thermal X-ray emission is seen to extend to large distances (5 to 20 kpc) above the planes of edge-on *starburst* galaxies (e.g. Fabbiano, Heckman & Keel 1990; Armus et al. 1995; Read, Ponman & Strickland 1997; Dahlem, Weaver & Heckman 1998), which also show unambiguous optical emission line evidence for energetic galactic scale outflows — “superwinds” (Heckman et al. 1990). These outflows are

potentially very significant in enriching and heating the IGM (Heckman 1999).

Both fully-numerical and semi-analytical theoretical modeling (Suchkov et al. 1994; Silich & Tenorio-Tagle 1998; Murakami & Babul 1999) suggest that the properties of the gaseous halos these winds expand into play a major role in determining the fate of the material in superwinds (i.e. escape into the IGM, or confinement and eventual return to the disk). Although simulations of starburst-driven winds should be treated with caution, given the lack of calibration against observational data, one robust result is the sensitivity of the wind properties (in particular mass and metal loss to the IGM) on the disk and halo ISM properties (e.g. De Young & Heckman 1994; Suchkov et al. 1994; Silich & Tenorio-Tagle 1998; Strickland & Stevens 2000; Silich & Tenorio-Tagle 2001). In our view, the emphasis given to galactic mass as a primary parameter influencing gas and metal ejection efficiencies (e.g. Dekel & Silk 1986; Mac Low & Ferrara 1999; Ferrara & Tolstoy 2000; Ferrara et al. 2000) blinds non-expert readers to the more fundamental role played by the poorly-known disk and halo ISM distributions. The gravitational potential only enters at a secondary level, by influencing the gas distribution and finally via the escape velocity. Redressing the lack of observational knowledge about the gaseous halos that superwinds must pass through is one motivation for studying the halos of *normal* star-forming galaxies.

Modern theories of the ISM in normal spiral galaxies also predict hot gas in the halo, due to the interchange of material between the disk and halo through “galactic fountains” (Shapiro & Field 1976; Bregman 1980; de Avillez 2000), or in a more-localized form through “chimneys” (Norman & Ikeuchi 1989). Energy feed back into the ISM from supernovae is believed to create bubbles of hot, metal-enriched, gas, which blow out of the disk and vent their contents into the halo of the galaxy. After $\gtrsim 10^8$ years or so, this material cools and falls back to the disk, possibly in a form analogous to the Galactic high velocity clouds.

Unfortunately, many of the fundamental aspects of these fountain/chimney disk/halo interaction theories are observationally unconstrained, fundamentally due to our *current* lack of knowledge about the X-ray properties of spiral galaxy halos. In the theoretical paradigm, fountains are primarily driven by the over-pressurized hot gas created by SNe, and the most direct diagnostic of the energetics, and elemental composition, of this gas is the thermal X-ray emission it

produces.

Studies of nearby edge-on star-forming galaxies with *Einstein* and the *ROSAT PSPC* revealed *only one* normal spiral, NGC 891 (Bregman & Pildis 1994), with X-ray-emitting gas in its halo⁴. Although edge-on normal spiral galaxies did not receive as much attention with *Einstein* & *ROSAT* as other classes of galaxy, those observations that were performed failed to produce believable detections of hot halo gas in other edge-on⁵ normal star-forming galaxies (Bregman & Glassgold 1982; Vogler, Pietsch & Kahabka 1995; Bregman & Houck 1997; Fabbiano & Juda 1997; Benson et al. 2000). X-ray studies of our own galaxy's halo and disk/halo interface (e.g. Kuntz & Snowden 2000) provide information complementary to the study of other galaxies, but are difficult to perform and interpret due to our location within the disk.

More progress on investigating the disk/halo interface in normal galaxies has been made at other wavelengths, primarily in the optical, where extra-planar H α emission (e.g. Dettmar 1992; Rand 1996; Hoopes, Walterbos & Rand 1999) and dust (Howk & Savage 1999) has been detected in a variety of nearby, normal spiral galaxies. These studies have shown that the presence of such tracers of disk/halo interaction increases with higher levels of star-formation intensity in the underlying disk, but the mechanisms behind these phenomena, and their energetics, are still unclear.

It is also not clear to what extent fountains are a distinct phenomenon from superwinds. It is not unreasonable to think that physical conditions and kinematics of the gas making up a fountain may be quite different from that in a superwinds, despite the general similarity in driving mechanism. For example, the filling factor of the dominant X-ray-emitting plasma might

⁴NGC 4631 is often presented as an example of a “normal” spiral galaxy with a X-ray-emitting halo (e.g. see Wang et al. 2001). However, its large-scale-height non-thermal radio halo, warm IRAS 60 to 100 μ m flux ratio, high H α luminosity and optically disturbed morphology all point to it being highly atypical. It is a good example of a galaxy experiencing a mild, disk-wide, starburst event (Golla & Wielebinski 1994). We believe that the *ROSAT PSPC*-based detection of a $L_X = 2.6 \times 10^{39}$ diffuse X-ray halo around NGC 4565, claimed by Vogler et al. (1995), is incorrect, as the archival 2.9 ksec *Chandra* ACIS-S observation (ObsID 404) reveals that the X-ray emission $\sim 2'$ east of the nucleus (that comprised the majority of the emission originally considered to be diffuse) is due to two point sources.

⁵Diffuse X-ray emission in approximately face-on star-forming galaxies (e.g. Snowden & Pietsch 1995; Cui et al. 1996; Ehle et al. 1998), can not be unambiguously associated with a hot halo, for obvious reasons.

be high in a fountain (Bregman 1980), as compared to superwinds where the filling factor is low (Chevalier & Clegg 1985; Suchkov et al. 1994; Strickland & Stevens 2000; Strickland et al. 2000). Another intriguingly hint of a difference comes from the *ROSAT PSPC*-based sample of both normal spiral galaxies and starburst galaxies of all inclinations by Read & Ponman (2001). They find that the X-ray-emitting gas “in the coronal systems [i.e. galaxies assumed to have a hydrostatic hot gas corona/halo] appears to be cooler than that seen in the wind systems [i.e. starburst galaxies with superwinds]”.

Practitioners of semi-analytical (e.g. Benson et al. 2000), and numerical cosmological models (e.g. Toft et al. 2002) of galaxy formation and evolution offer a radically different origin for X-ray emitting halos around spiral galaxies. Inter-galactic gas continually flows into galactic halos, is heated in an accretion shock to the halo virial temperature (although Katz et al. 2002 argue that accreted gas may remain cool), and then cools and accretes onto the disk. These models predict red-shift zero spiral galaxy X-ray luminosities at, or just below, the *ROSAT*-based observational upper limits. The predicted X-ray luminosity is a strong function of the galaxy mass, $L_X \propto v_{\text{rot}}^5$, and that the temperature of the gas is similar to the halo virial temperature $kT \sim 0.5 \mu m_H v_{\text{rot}}^2$. The majority of the diffuse X-ray emission arises close to the disk, the X-ray surface brightness dropping off semi-exponentially with height above the disk. These halo properties should be largely independent of the host disk's SF intensity, and the exact numerical implementation of SN feedback (J. Sommer-Larsen, 2002, private communication).

In order to investigate some of these questions we have compiled a sample of 10 edge-on star-forming galaxies which have both ground-based narrow-band optical imaging (probing extra-planar gas at $T \sim 10^4$) and X-ray observations with the *Chandra* X-ray Observatory. The spatial resolution of the *Chandra* telescope ($\sim 0.^{\prime\prime}8$ FWHM) is an order of magnitude better than any previous or currently-existing X-ray instrument. As approximately half of the X-ray luminosity of a star-forming galaxies is due to X-ray luminous point sources, accurate studies of the X-ray diffuse emission require high spatial resolution in order to allow point source removal.

In Strickland et al. (2003, henceforth referred to as Paper I) we described the sample, the X-ray and optical data reduction performed, and presented results and interpretation of a spatial and spectral analysis of

TABLE 1
BASIC PHYSICAL PROPERTIES OF THE SAMPLE GALAXIES

Galaxy	α, δ (J2000) (h m s, ° ' '')	i (°)	PA (°)	v_{rot} (km/s)	D (Mpc)	scale (pc)	f_{60} (Jy)	f_{60}/f_{100}	$L/(10^{10} L_{\odot})$			$L_{H\alpha}$ ($10^{40} \text{ erg s}^{-1}$)	M_{TF} ($10^{10} M_{\odot}$)
(1)	(2)	(3)	(4)	(5)	(6)	(7)	(8)	(9)	(L_{IR}) (10)	(L_{K}) (11)	(L_{B}) (12)	(13)	(14)
M82	09 55 51.9 +69 40 47.1 ^a	73 ^b , 82 ^c	65 ^d	137 ^a	3.6 ^e	17.5	1313.5 ^f	0.97	5.36	0.75	0.33	7.0 ^g	1.9
NGC 1482	03 54 39.3 -20 30 08.9 ^h	58 ⁱ	103 ^j	165 ^k	22.1	107.1	35.3 ^f	0.77	5.00	0.84	0.38	N 9.4 ^l	3.7
NGC 253	00 47 33.2 -25 17 16.2 ^m	79 ⁿ , 72 ^o	52 ^d , 49 ^p	225 ^m	2.6 ^p	12.6	936.7 ^f	0.50	2.10	0.89	0.58	3.6 ^q	10.6
NGC 3628	11 20 16.95 +13 35 20.1 ^r	87 ^s , 80 ^r	104 ^d	229 ^f	10.0 ^u	48.5	51.6 ^f	0.50	1.74	1.58	1.06	N 2.3 ^v	11.3
NGC 3079	10 01 57.8 +55 40 47.2 ^w	85 ^w	165 ^d	244 ^f	17.1	82.9	50.2 ^f	0.49	4.76	1.55	0.98	N 9.1 ^d	14.1
NGC 4945	13 05 25.3 -49 29 09.0 ^x	78 ^y	43 ^y	184 ^f	3.7	17.9	588.1 ^z	0.42	2.70	0.94	0.73	N 2.4 ^d	5.2
NGC 4631	12 42 07.2 +32 32 31.9 ^{aa}	85 ^{ab} , 81 ^{ac}	86 ^{ac} , 83 ^{ac}	150 ^{ab}	7.5 ^{ab}	36.4	82.9 ^z	0.40	1.74	0.62	0.98	N 14.3 ^{ad}	2.6
NGC 6503	17 49 26.4 +70 08 39.7 ^{ae}	75 ^{af}	123 ^{af}	120 ^{ag}	5.2 ^{ah}	25.2	10.2 ^f	0.35	0.12	0.14	0.18	0.76 ^{ai}	1.2
NGC 891	02 22 33.2 +42 20 56.2 ^{aj}	89 ^{aj}	23 ^{aj}	225 ^f	9.6	46.5	61.1 ^z	0.31	2.47	1.66	0.78	3.3 ^{ge}	10.6
NGC 4244	12 17 29.7 +37 48 20.4 ^{ak}	85 ^{ak}	48 ^{ak}	100 ^{ak}	3.6	17.5	4.2 ^z	0.26	≤ 0.02	0.04	0.08	0.42 ^{ad}	0.6

NOTE.—Column 2: Coordinates of the dynamical center of the galaxy, where available. Column 3: Inclination. Column 4: Position angle of the galactic disk. Multiple values for the inclination and position angle are given when several values are often reported in the literature. Column 5: Inclination-corrected circular velocity within the disk. Column 6: Assumed distance. Unless a specific reference is given, distances were calculated using the galaxy recessional velocity with respect to the microwave background (de Vaucouleurs et al. 1991), and $H_0 = 75 \text{ km s}^{-1} \text{ Mpc}^{-1}$. Column 7: Physical distance corresponding to an angular size of 1 arcsecond. Column 8: IRAS 60/ μm flux in Janskys. Column 9: IRAS 60 to 100/ μm flux ratio. Column 10: Total IR luminosity based on the observed IRAS fluxes, $L_{\text{IR}} = 5.67 \times 10^5 D_{\text{Mpc}}^2 \times (13.48f_{12} + 5.16f_{25} + 2.58f_{60} + f_{100}) L_{\odot}$, where D_{Mpc} is the distance to the galaxy in Mpc (Sanders & Mirabel 1996). The exact source of the IRAS data used is given in a case by case basis above. Where multiple measurements were available for any galaxy, we used the following sources in order of preference: Rice et al. (1988), and Soifer et al. (1989). Column 11: K-band luminosity, calculated from the K-band total magnitudes given in Jarret et al. (2003) and converted to the Cousins-Glass-Johnson system using the transformations presented in Carpenter (2001). Zero points for conversion from magnitude to flux were taken from Bessel, Castelli & Plez (1998). Note that the units are L_{\odot} , not $L_{\text{K},\odot}$. Column 12: B-band luminosity from RC3 catalog B_T magnitude (de Vaucouleurs et al. 1991), and corrected for Galactic extinction using reddening values from Burstein & Heiles (1982). Note that no correction for extinction internal to the specific galaxy has been made. Column 13: Observed H α -luminosity in units of $10^{40} \text{ erg s}^{-1}$. Note these values have *not* been corrected for extinction. Measurements that have not been corrected for [NII] emission are marked with a preceding *N*. Column 14: Baryonic mass (stellar plus H I) estimated from the K-band Tully Fisher relationship of Bell & de Jong (2001), where $M_{\text{TF}} = 10^{9.79} \times (v_{\text{rot}}/100 \text{ km s}^{-1})^{3.51} M_{\odot}$.

REFERENCES.—(a) Welischew, Fomalont & Greisen (1984), (b) Ichikawa et al. (1995), (c) Lynds & Sandage (1963), (d) Lehnert & Heckman (1995), (e) Freedman et al. (1994), (f) Soifer et al. (1989), (g) McCarthy, Heckman & van Bruegel (1987), (h) 2MASS Second Incremental Release, (i) Hameed & Devereux (1999), (k) Calculated assuming $v_{\text{rot}} = W_{20}/2 \sin^2 i$, using the W_{20} value from Roth, Mould & Davies (1991), (l) Hameed & Devereux (1999), (m) Sorai et al. (2000), (n) Pence (1981), (o) Puche, Carignan & van Gorkom (1991), (p) Puche & Carignan (1988), (q) From H α images published in Strickland et al. (2002a), (r) Douglas et al. (1996), (s) Irwin & Sofue (1996), (t) Sofue (1997), (u) Soifer et al. (1987) (v) Fabbiano et al. (1990), (w) Irwin & Seaquist (1991), (x) Ott et al. (2001), (y) Koorneef (1993), (z) Rice et al. (1988), (aa) Dynamical center, Golla & Wielebinski (1994), (ab) Rand (1994), (ac) Golla (1999), (ad) Hoopes et al. (1999), (ae) Central optical & X-ray source, Lira, Johnson & Lawrence (2002), (af) de Vaucouleurs et al. (1991), (ag) Bottema & Gerritsen (1997), (ah) Karachentsev & Sharina (1997), (ai) Kennicutt (1998a). (aj) Nuclear 1.4 GHz continuum point source, Rupen (1991), (ak) H I dynamical center, Olling (1996).

the diffuse X-ray emission.

In this paper we investigate how the empirical properties of the hot gas, in particular gas in the halos of these galaxies, correlate with the size, mass, star formation rate and star formation intensity in the host galaxies. From this analysis we investigate various aspects of mechanical energy “feedback” — the return of energy to the ISM from massive star supernovae and stellar winds — on galactic scales.

We describe the sample and their star-formation properties in § 2. In § 3 we provide a brief summary of the results from Paper I, before moving onto considering what correlations exist between the properties of the diffuse X-ray emission and other multi-wavelength properties of the galaxies in § 4. In § 5 we discuss these results with respect to various aspects of feedback-related theory, in particular the conditions necessary for blow-out of gas from the disk and halo, and the fraction of supernova mechanical energy available to drive large-scale ISM motions. Our results and conclusions are summarized in § 6.

2. Sample galaxies

The sample is formed of seven starburst galaxies and three “normal” star-forming galaxies, all approximately edge-on ($i \gtrsim 60^\circ$) moderate luminosity ($L_{\text{BOL}} \sim 10^{10} L_\odot$), moderate-mass ($M \sim 10^{10} - 10^{11} M_\odot$) disk galaxies within a distance of $D \lesssim 20$ Mpc. This sample contains all the disk galaxies for which *Chandra* ACIS data was available to us as of 2002 September, including both public data and our own propriety observations.

Basic physical properties of the sample galaxies are shown in Table 1. We distinguish between starburst galaxies and more-normal star-forming galaxies on the basis of their IR-warmth — specifically the IRAS 60 to 100 μm flux ratio f_{60}/f_{100} . Higher star formation rates per unit disk area lead to higher dust temperatures, and hence higher f_{60}/f_{100} ratios, with starburst galaxies typically having $f_{60}/f_{100} \geq 0.4$. We will refer to those galaxies with $f_{60}/f_{100} < 0.4$ as the normal spirals. We refer the reader to Paper I for a more detailed discussion of the sample and the distinction between starburst and normal spiral galaxies.

Intuitively, we would expect the effect of mechanical energy feedback on the galactic scale to depend on the total star formation rate, and/or the star formation rate per unit volume or area. Star formation and supernova rates for the sample galaxies are given in Table 2.

Note that galaxies are listed in all tables in order of decreasing f_{60}/f_{100} ratio, *i.e.* approximately in order of decreasing star formation rate per unit area.

2.1. Star formation rates and intensities

We also consider two other simple, and widely-available proxies of the star-formation intensity: FIR and non-thermal radio face-on surface brightnesses, quantified for our sample in Table 2. Although somewhat simplistic estimators of SF intensity, these do have the advantages of being available for almost all local disk galaxies from uniformly-obtained datasets, and are distance-independent.

Very detailed studies of the star-formation rates, spatial distributions, and history, are available for the brightest starbursts such as M82 (Rieke et al. 1993; McLeod et al. 1993; Satyapal et al. 1997; de Grijs, O’Connell & Gallagher 2001; Förster Schreiber et al. 2001) and NGC 253 (Engelbracht et al. 1998), but measurements of similar quality are not available for many of the starburst galaxies in our sample, let alone the normal spiral galaxies. We did calculate star formation intensities for all our sample galaxies based on all available optical, NIR and radio measurements we could find in the literature, but found the scatter in estimated SF intensity for any particular galaxy to be intolerably large.

The FIR luminosity divided by the optical isophotal diameter (in kpc) at 25th magnitude, L_{FIR}/D_{25}^2 , is often used as a proxy for the mean star-formation rate per unit disk area in spiral galaxies (we shall occasionally refer to the star formation rate per unit disk area as the SFRI for convenience). The presence of extra-planar H α and/or radio emission, and extra-planar dust, is known to qualitatively correlate with this parameter (Rand 1996, see also Dettmar 1998; Howk & Savage 1999; Rossa & Dettmar 2000; Dahlem et al. 2001). It under-estimates the true SF intensity in starburst galaxies, as the star-formation is often much more concentrated than the old stellar light measured by D_{25} . This method also over-estimates the mean SF intensity in galaxies with star-formation rates somewhat less than that of the Milky Way, where an increasing fraction of L_{FIR} is due to cool dust heated by diffuse star-light, and not by massive stars.

Non-thermal radio emission, due to synchrotron emission from relativistic electrons accelerated in supernova remnants, provides a good tracer of SF activity on galactic scales (Condon 1992). The 1.4 GHz

TABLE 2
STAR-FORMATION AND SUPERNOVA RATES, SF INTENSITY, AND PROXIES THEREOF

Galaxy	$SFR_{H\alpha,T}$	$SFR_{IR,T}$	D_{25}^i	K-band $r_{0.5}$	f_{FIR}	f_{FIR}/D_{25}^2	$F_{\text{SN,FIR},D_{25}}$	$\mathcal{R}_{\text{SN},T}$	$f_{1.4\text{GHz}}$	$L_{1.4\text{GHz}}$	$\theta_{1.4\text{GHz}}$	$f_{1.4\text{GHz}}/4\theta_{1.4\text{GHz}}^2$	$F_{\text{SN,FIR},\theta_{1.4\text{GHz}}}$	$\log \tau_{\text{gas}}$	$\log \mu$			
(1)	(2)	(3)	(4)	(5)	(6)	(7)	(8)	(9)	(10)	(11)	(12)	(13)	(14)	(15)	(16)	(17)	(18)	(19)
M82	> 0.55	9.2	8.9	9.3	0.69	0.72	4745.9	16.60	1211.0	0.107	7386.8	5.47×10^4	14.8	0.26	8.41	4.0×10^5	2.04	8.34
NGC 1482	> 0.74	8.6	2.2	14.1	0.10	0.66	136.8	7.93	503.0	0.100	236.7	7.91×10^4	11.3	1.21	0.46	1.7×10^4	1.74	8.27
NGC 253	> 0.28	3.6	20.4	15.4	3.56	2.69	4288.3	2.86	177.1	0.042	5704.5	1.38×10^4	29.1	0.37	1.69	7.8×10^4	2.11	8.65
NGC 3628	> 0.18	3.0	10.5	30.5	1.67	4.86	244.5	0.606	37.5	0.035	470.2	1.98×10^4	20.9	1.01	0.27	8.5×10^3	2.33	8.08
NGC 3079	> 0.72	8.1	5.5	27.4	0.71	3.54	232.8	2.14	127.1	0.129	820.7	1.53×10^5	18.3	1.52	0.61	1.4×10^4	2.62	8.27
NGC 4945	> 0.19	4.6	13.8	14.9	2.88	3.09	2927.7	4.28	246.5	0.054	4200.0	3.92×10^4	30.0	0.54	4.47	1.9×10^5	2.88	8.37
NGC 4631	> 1.13	3.0	10.5	22.9	1.51	3.29	412.3	1.07	66.8	0.035	771.7	1.71×10^4	59.6	2.17	0.0543	1.9×10^3	2.48	7.70
NGC 6503	> 0.06	0.20	5.6	8.4	0.77	1.18	55.1	0.492	16.7	0.0012	41.9	6.74×10^2	34.6	0.87	0.0088	4.0×10^2	2.97	8.23
NGC 891	> 0.26	4.2	9.3	26.1	1.47	4.10	355.6	1.14	39.5	0.049	285.7	1.50×10^4	55.2	2.57	0.0234	1.9×10^3	3.19	8.19
NGC 4244	> 0.03	0.04	10.2	10.7	1.85	1.94	27.2	0.071	3.5	0.0004	20.3	5.65×10^1	158.5	2.84	0.0003	1.2×10^1	4.53	7.72

NOTE.—Column 2: Lower limits on the total galactic star formation rate ($M_{\odot} \text{ yr}^{-1}$), based on the $H\alpha$ luminosity and using the formulae given in Kennicutt (1998b). Note that no correction for extinction has been applied. Column 3: Estimated total galactic star formation rate ($M_{\odot} \text{ yr}^{-1}$), based on the IR luminosity, where $SFR_{IR} = 4.5 \times 10^{-44} L_{IR} [\text{erg s}^{-1}]$, again using the Kennicutt (1998b) formulae. Columns 4 and 5: Inclination-corrected diameter of the stellar disk in arcminutes (4) and kpc (5), based on the D_{25} values given in the RC3 and the distances given in Table 1. The method of Tully & Fouqué (1985) was used to correct the observed D_{25} values for inclination. Columns 6 and 7: K-band half light radii in arcminutes (6) and kpc (7). Original values were taken from the 2MASS Large Galaxy Atlas (Jarret et al. 2003). Column 8: IRAS Far-IR flux $f_{\text{FIR}} = 2.58 \times f_{60} + f_{100}$, in Jy. To convert to units of $\text{erg s}^{-1} \text{ cm}^{-2}$ multiply by 1.26×10^{-11} . Column 9: Far-IR luminosity per unit stellar disk area f_{FIR}/D_{25}^2 , in distance-independent units of mJy arcsec^{-2} . To convert to the commonly used units of $10^{40} \text{ erg s}^{-1} \text{ kpc}^{-1}$ multiply f_{FIR}/D_{25}^2 by 6.484. Column 10: One estimate of the mean galactic supernova rate per unit area, $F_{\text{SN,FIR},D_{25}} = \mathcal{R}_{\text{SN}}/D_{25}^2$, in units of $\text{SN Myr}^{-1} \text{ kpc}^{-2}$, is based on the star-formation rate calculated from L_{IR} . Column 11: Estimated total galactic core-collapse supernova rate (yr^{-1}), where $\mathcal{R}_{\text{SN}} = 0.2L_{IR}/10^{11} L_{\odot}$ (Heckman et al. 1990). Column 12: 1.4 GHz radio flux in mJy, based on the NVSS data. See § 2.2 for more details. Column 13: 1.4 GHz luminosity in units of Solar luminosities, where $L_{1.4\text{GHz}} = 4\pi D^2 \nu f_{1.4\text{GHz}}$. The major-axis half-light radius, in units of arcseconds and kpc, that we derive the NVSS data is given in columns 14 and 15 respectively. Column 16: Effective 1.4 GHz surface brightness, in mJy arcsec^{-2} . Column 17: Another estimate of the mean SN rate per unit area $F_{\text{SN,FIR},\theta_{1.4\text{GHz}}} = \mathcal{R}_{\text{SN}}/4\theta_{1.4\text{GHz}}^2$ (again in units of $\text{SN Myr}^{-1} \text{ kpc}^{-2}$), based on the star-formation rate calculated from L_{IR} but using NVSS-based size $\theta_{1.4}$. Note that NGC 4945 was not observed in the NVSS. For NGC 4945 we use the nuclear region 1.4 GHz flux and size from Elmoutouf et al. (1997), whose observations had similar spatial resolution to that of the NVSS. Column 18: Logarithm of the gas consumption timescale in Myr, where $\log \tau_{\text{gas}} = \log \Sigma_{\text{gas}} - \log \Sigma_{\text{SFR}}$, and Σ_{gas} and Σ_{SFR} are the surface density of gas ($M_{\odot} \text{ pc}^{-2}$) and star-formation rate ($M_{\odot} \text{ yr}^{-1} \text{ pc}^{-2}$) respectively. Data are from Kennicutt (1998a), except for NGC 1482, NGC 3628, NGC 4244, NGC 4631 and NGC 4945. For these galaxies the star formation rate was estimated from the IRAS fluxes. Gas masses were obtained from Elfhag et al. (1996) for NGC 1482 (using the CO brightness to H_2 column density scaling in Kennicutt (1998a), and a radius of 2 kpc, as ISO observations by Dale et al. (2000) demonstrate that 80% of the star-formation occurs within this radius), Irwin & Sofue (1996) for NGC 3628 (central, $R \leq 340$ pc, H_2 gas mass), from Olling (1996) for NGC 4244 (total HI gas mass), from Golla & Wielebinski (1994) for NGC 4631 (H_2 gas mass for $R \leq 2.5$ kpc) and from Dahlem et al. (1993) for NGC 4945 (molecular gas mass within central 1.1 kpc). Column 19: Logarithm of the mean mass surface density $\mu = M_{\text{TF}}/D_{25}^2$.

luminosity of a galaxy is almost directly proportional to the SF rate, which, combined with the measured angular size of the radio-emitting region, provides a good SF intensity measurement (Dahlem et al. 2001).

The radio fluxes, sizes and SF intensity values given in Table 2 are based on 1.4 GHz images from the NRAO/VLA Sky Survey (NVSS, see Condon et al. 1998), with the exception of southern galaxy NGC 4945, which lies outside the region of sky surveyed by the NVSS. A description of how these values were obtained is given in § 2.2

2.2. Radio fluxes, sizes and SF intensity measurements

Radio fluxes and half-light radii were measured from the processed NVSS 1.4 GHz radio images (<http://www.cv.nrao.edu/nvss/postage.shtml>). Fluxes were summed within rectangular apertures encompassing the optical disk of each galaxy, each of total width equal to the optical D_{25} diameter and breadth equal to the minimum of 1.5 (twice the angular resolution of the NVSS) or the angular equivalent of 4 kpc, and centered on the nuclear positions given in Table 1. The major-axis half-light radii $\theta_{1.4}$ were measured from the radio flux within the disk regions defined above using $\Delta r = 5''$ -wide pixels. Inspection of the resulting radio surface brightness slices demonstrated that the fluxes at the extreme ends of the slices were in all cases statistically consistent with zero, allowing us to define the 100%-enclosed light radii as the edges of the surface brightness profiles. Given the linear, rather than radial, nature of these major-axis surface brightness profiles we obtained two half-light radii on either side of the nucleus for each galaxy, θ_{+r} and θ_{-r} , which were combined to give the final half light radius $\theta_{1.4} = \{(\theta_{+r}^2 + \theta_{-r}^2)/2\}^{1/2}$ shown in Table 2.

We did not use the fluxes and sizes given in the NVSS Source Catalog itself, which quotes fluxes and sizes from a 2-dimensional Gaussian model fit to the radio images. The NVSS Source Catalog underestimates the total 1.4 GHz flux from galaxies such as NGC 253, NGC 3628 and NGC 4631 by a factor ~ 2 , where a relatively bright compact nuclear region of radio emission is surrounded by a fainter extended radio-emitting disk, *i.e.* cases where a single Gaussian fit to the flux distribution does not work well.

NGC 4945 is a southern hemisphere target and hence was not observed in the NVSS. For NGC 4945 we use the nuclear region 1.4 GHz flux and size quoted

in Elmouttie et al. (1997). Their observations had a similar spatial resolution to that of the NVSS, making these values a reasonably good match to the values we use for the other galaxies.

Note that the moderately-low spatial resolution of this radio data (FWHM = 45'') will over-estimate the spatial size of the radio emission for the more compact starbursts (and hence under-estimate the SF intensity), especially for the more distant galaxies such as NGC 3079 and NGC 1482.

3. Summary of results from Paper I

In Paper I (Strickland et al. 2003) we presented a detailed study of the diffuse X-ray emission in a sample of 10 approximately edge-on disk galaxies (7 starburst galaxies, 3 normal spirals) that span the full range of star formation found in disk galaxies. With the arc-second spatial resolution of the *Chandra* X-ray telescope we were able to separate the X-ray emission from point sources from the truly diffuse component. The high spatial resolution also allowed a meaningful comparison to be made of the spatial location of the X-ray emission with respect to multi-wavelength data (in particular to ground or space-based optical imaging). In addition to a detailed discussion of each galaxy, we presented a mini-atlas of soft and hard X-ray, H α and R-band images of each of the 10 galaxies, shown at a common spatial and surface brightness scale to facilitate cross-comparison.

We presented a variety of quantitative measures of the spatial extent, spectral hardness, and shape of the diffuse X-ray emission, several of which can be applied to future samples of galaxies with lower S/N data. We found that the spectral properties of the diffuse X-ray emission show only weak, or some cases no, variation with increasing height (outside a heavily-absorbed, spectrally-harder region within $z \sim 2$ kpc of the disk mid-plane). The vertical decrease in surface brightness of the extra-planar emission ($|z| \geq 2$ kpc) appears to better described by exponential (effective surface brightness scale heights are typically between 2 – 4 kpc), or Gaussian models, than the power law expected of a freely expanding fluid.

For the eight galaxies with detections of extra-planar (*i.e.* halo-region) diffuse emission, we find that a common spectral model, comprising a two-temperature MEKAL (Mewe et al. 1995) hot plasma model with an enhanced α -to-Fe element ratio, can simultaneously fit the ACIS X-ray halo-region spec-

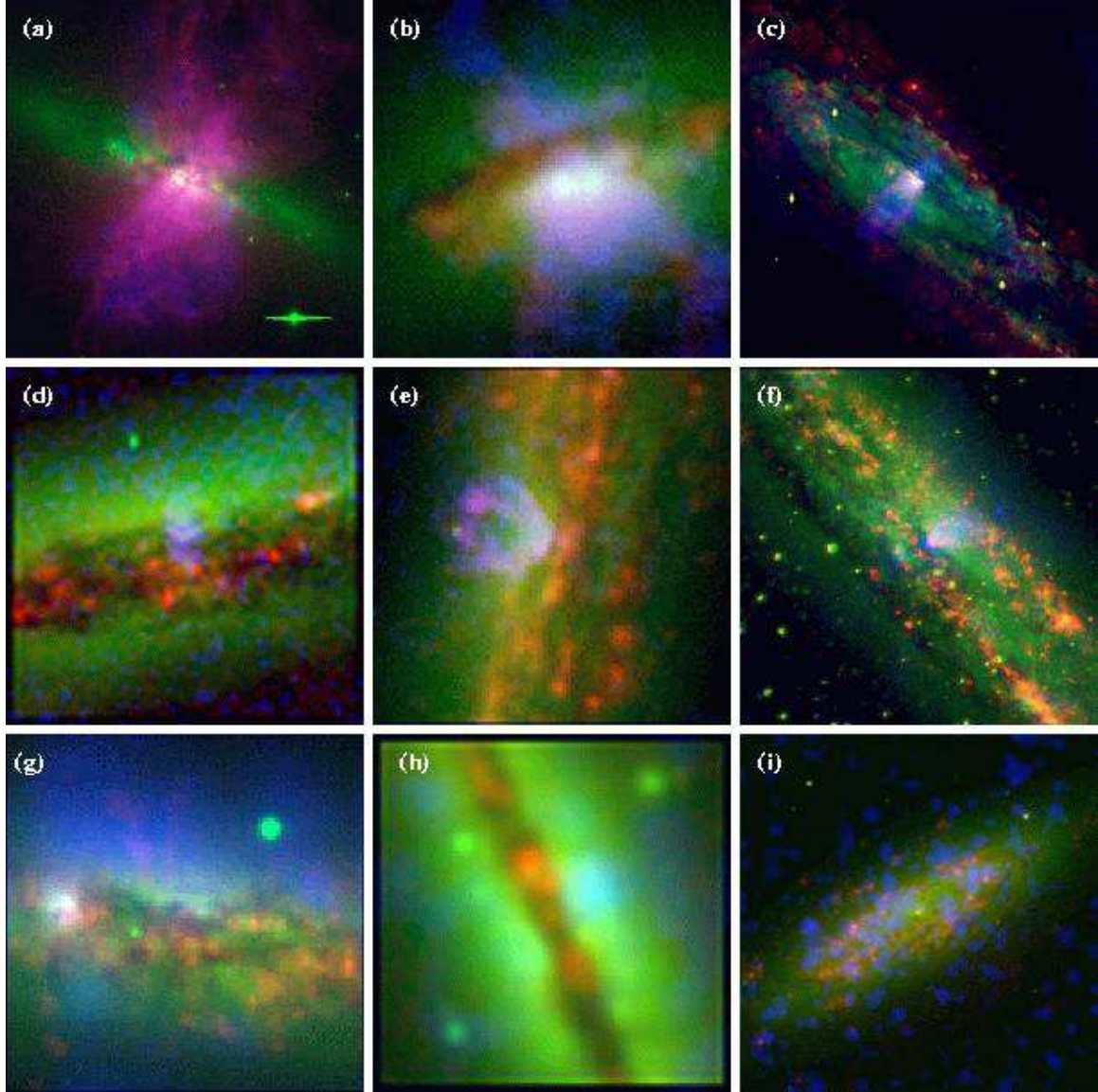


Fig. 1.— False color composite images of the central 5 kpc by 5 kpc of M82 (a), NGC 1482 (b), NGC 253 (c), NGC 3628 (d), NGC 3079 (e), NGC 4945 (f), NGC 4631 (g), NGC 891 (h) and NGC 6503 (i). H α emission is shown in red, optical R-band in green and 0.3–2.0 keV energy band soft X-ray emission is shown in blue. The X-ray emission is the point-source subtracted diffuse emission which has been adaptively smoothed to achieve a local S/N of 3, which tends to over-smooth structure in the X-ray emission. All images are shown on a square-root intensity scale. In contrast to Figs. 2 to 13 presented in Paper I, the same absolute intensity is not used, in order to show some of the fainter emission features. The galaxies are shown in order of (approximately) decreasing star formation rate per unit area. Note the close spatial similarities between the minor-axis-oriented H α emission and the diffuse X-ray emission, in particular the limb-brightened outflow cones in NGC 1482, NGC 253, NGC 3079 and NGC 4945.

tra. The X-ray-derived metal abundances show super-Solar ratios of α -process elements (primarily oxygen) to iron. This is consistent with the origin of the X-

ray emission being either (metal-enriched) merged SN ejecta, or from shocked ambient halo ISM (with moderate depletion of refractory elements onto dust).

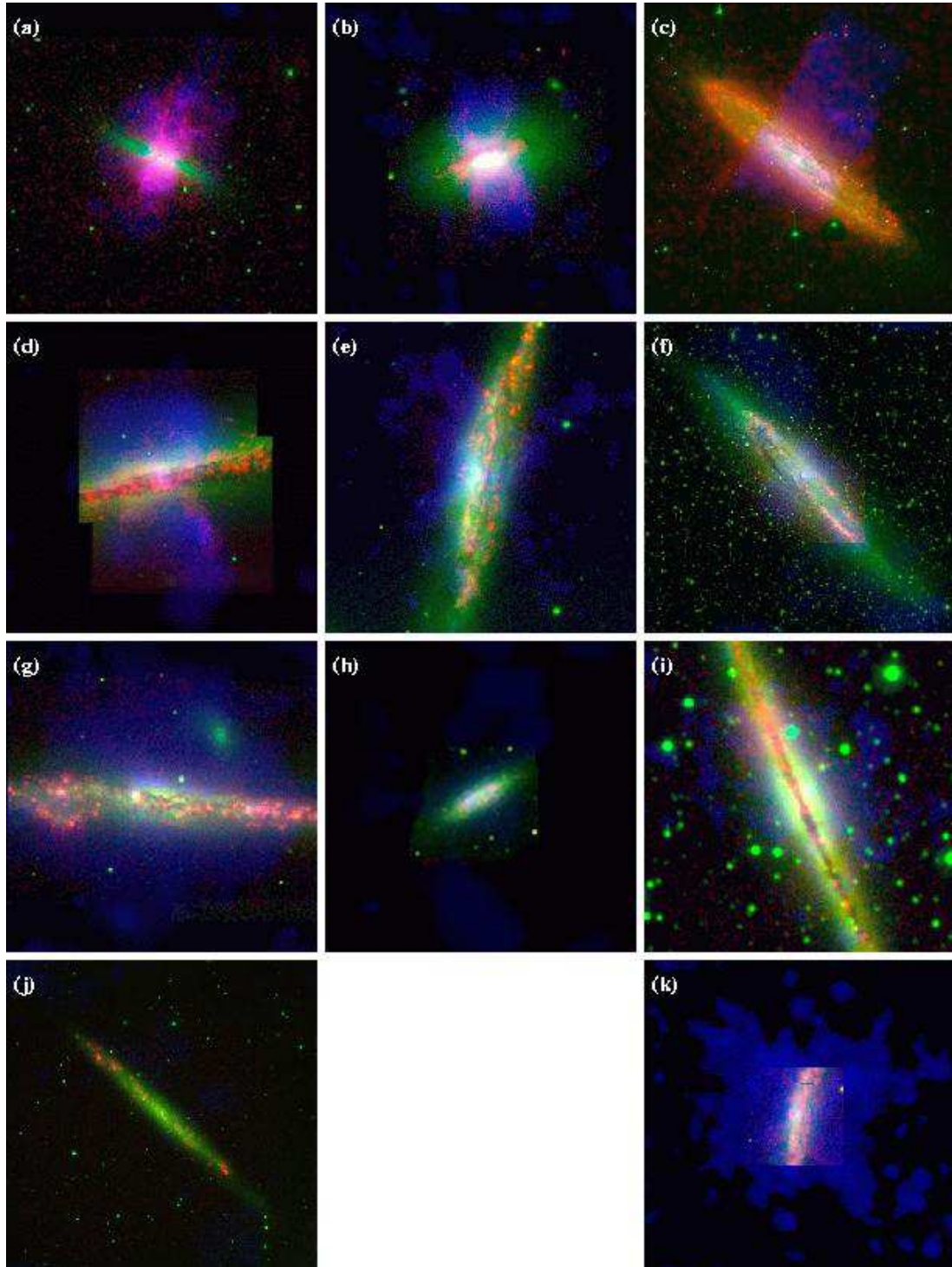


Fig. 2.— As Fig. 1, except that panels (a) through (j) now show 20 kpc by 20 kpc boxes, while in panel (k) the region is 40 kpc by 40 kpc. The galaxies are M82 (a), NGC 1482 (b), NGC 253 (c), NGC 3628 (d), NGC 3079 (e and k), NGC 4945 (f), NGC 4631 (g), NGC 6503 (h), NGC 891 (i), NGC 6503 (j), and NGC 3079 (k).

Our favored model for the origin of the extra-planar soft X-ray emission is that SN feedback in the disks of star-forming galaxies create, via blow out and venting of hot gas from the disk, tenuous exponential atmospheres of density scale height $H_g \sim 4 - 8$ kpc. AGN-driven winds do not appear to be significant in this sample, in that there is no obvious correlation between the presence and luminosity of any AGN and the properties of the diffuse X-ray emission. The soft thermal X-ray emission observed in the halos of the starburst galaxies is either pre-existing halo medium (which has been swept-up and shock-heated by the starburst-driven superwinds) or from a small fraction (by volume) of the merged-SN-ejecta that has been compressed near the walls of the outflow (e.g. by a reverse shock propagating back into the outflowing wind). In either case the observed exponential X-ray surface brightness distributions are an inheritance from galactic fountain activity prior to the currently-observed starburst phase. This model is based on the qualitative 2-D morphology of the diffuse X-ray and optical H α emission (in particular the filamentary, occasionally limb-brightened morphology of both the X-ray and H α emission), as well as interpretation of the more-quantitative minor axis surface brightness and spectral hardness profiles. An implication of this model is that galactic-scale gaseous halos may be common around star-forming disk galaxies. Observing starburst galaxies, in which superwinds “light-up” these pre-existing halos, may present the best method for studying the gaseous halos of star-forming galaxies.

4. Correlation analysis

We shall now move onto a more-quantitative comparison of the properties of the diffuse X-ray with other properties of host galaxies. For convenience, definitions of the data values we use (from both Paper I and this paper), the table numbers from which they were extracted, and the figures in which they are used, are given in Table 3

Given the very significant absorption of the diffuse emission from NGC 4945 by the high Galactic foreground hydrogen, the low detection significance and atypical spectral hardness of the halo diffuse emission (see Paper I), we have excluded it from further analysis. In particular, it is excluded from Figs. 3 to Fig. 8.

4.1. Star-formation or galaxy mass? The physical-drivers of extra-planar X-ray emission

The only previous study quantitatively comparing the *diffuse* X-ray emission⁶ from late-type, star-forming galaxies with their integrated luminosities at other wavelengths is the *ROSAT* PSPC-based study published in Read et al. (1997) and Read & Ponman (2001). They find that the estimated total diffuse emission X-ray luminosity per unit galaxy mass (estimated from L_X/L_B) correlates well with L_B , an estimator of galaxy mass for *normal* spirals. For starburst galaxies L_X/L_B shows a better correlation with L_{FIR} , *i.e.* with a proxy of star formation rate.

There are a number of reasons while it is worthwhile to re-examine this issue, apart from the obvious advantage of using the higher quality data from an instrument with greater sensitivity, and vastly superior capabilities of separating point-source and diffuse emission. Determining the properties of extra-planar hot gas in normal galaxies has assumed a new significance, given its importance as a diagnostic of the accuracy of theories of galaxy formation and evolution. The normal galaxy sample of Read & Ponman (2001) is largely a collection of face-on systems, with the approximately Milky-Way-like galaxy NGC 891 (van der Kruit 1984; Wainscoat et al. 1987) being classed as a starburst on the basis of the reddening-correction-sensitive $L_{\text{FIR}} > 0.38L_B$ criterion used by Read & Ponman as the definition of a starburst. It is only in high inclination systems where we can separate the disk and halo diffuse components, the latter being the most interesting component in testing both SN feedback models and cosmological accretion models.

There are only three approximately edge-on normal spiral galaxies in our sample, two of them being lower mass and lower luminosity than the average spiral. Nevertheless we are still able to determine how closely the properties of the diffuse X-ray emission in these systems resemble those of the edge-on starburst galaxies. Determining the properties of any extra-planar hot gas in the *average* normal spiral will require more observational time to be allocated to edge-on spiral galaxies.

⁶Significant effort has been expended in the past comparing the multi-wavelength luminosities of galaxies in an attempt to elucidate the physical causes of the *integrated* X-ray emission in these systems. We refer the interested reader to Fabbiano (1989), Shapley, Fabbiano & Eskridge (2001) and Fabbiano & Shapley (2002).

TABLE 3
SUMMARY AND LOCATION OF DATA VALUES USED IN THIS PAPER

Value (1)	Tabulated in (2)	Description (3)	Appears in (4)
Data values tabulated in this paper.			
L_{IR}	Table 1	Total galactic IR luminosity, derived from <i>IRAS</i> fluxes.	Figs. 3 and 4
L_K	Table 1	Total galactic K-band luminosity, derived from fluxes in the 2MASS Large Galaxy Atlas.	Figs. 3 and 4
L_B	Table 1	Total galactic B-band luminosity. Not corrected for extinction.	Figs. 3 and 4
v_{rot}	Table 1	Inclination-corrected peak circular velocity.	Figs. 5, 6 and 7
f_{60}/f_{100}	Table 1	IRAS 60 to 100 μm flux ratio, an indicator of the intensity of star formation.	Figs. 5 and 7
M_{TF}	Table 1	Galactic baryonic mass derived from the K-band Tully-Fisher relation.	Figs. 4 and 8
$L_{1.4\text{GHz}}$	Table 2	Total galactic radio luminosity at 1.4 GHz, derived from the NVSS.	Figs. 3 and 4
$f_{1.4\text{GHz}}$	Table 2	Total galactic radio flux at 1.4 GHz, derived from the NVSS.	...
$\theta_{1.4\text{GHz}}$	Table 2	Radio major-axis half light radius.	Fig. 6
$f_{1.4\text{GHz}}/\theta_{1.4\text{GHz}}^2$	Table 2	Radio-based estimate of the star formation rate intensity.	Figs. 5 and 7
f_{FIR}	Table 2	Total galactic IRAS FIR flux.	...
D_{25}	Table 2	Inclination corrected optical diameter at a surface brightness of 25 magnitudes per square arcsecond.	Fig. 6
f_{FIR}/D_{25}^2	Table 2	Commonly used proxy of the mean galactic star formation rate per unit area.	Figs. 5 and 7
K-band $r_{0.5}$	Table 2	K-band half light radius, from the 2MASS Large Galaxy Atlas.	Fig. 6
μ	Table 2	Mean galactic mass surface density.	Fig. 6
\mathcal{R}_{SN}	Table 2	Total galactic core-collapse supernovae rate, based on the total IR luminosity.	...
$F_{\text{SN,FIR,D}_{25}}$	Table 2	One estimate of the mean supernovae rate per unit disk area, where $F_{\text{SN,FIR,D}_{25}} = \mathcal{R}_{\text{SN}}/D_{25}^2$	Fig. 8
$F_{\text{SN,FIR},\theta_{1.4\text{GHz}}}$	Table 2	Another estimate of the mean supernovae rate per unit disk area, where $F_{\text{SN,FIR},\theta_{1.4\text{GHz}}} = \mathcal{R}_{\text{SN}}/4\theta_{1.4\text{GHz}}^2$	Fig. 8
Data values tabulated in Paper I.			
$\Sigma_{0.5}$	Table 4	Mean diffuse X-ray surface brightness between $z = 0$ and the minor half light height $z_{0.5}$ and between $-5 \leq r(kpc) \leq 5$.	Fig. 7
z_{1e-9}	Table 4	Height along the minor axis at which the diffuse X-ray surface brightness reaches $10^{-9} \text{ photons s}^{-1} \text{ cm}^{-2} \text{ arcsec}^{-2}$.	Fig. 8
$z_{0.95}$	Table 4	Minor axis diffuse X-ray 95%-flux enclosed height.	Fig. 8
$r_{0.5}$	Table 5	Major-axis diffuse X-ray half light radius.	Fig. 6
$r_{0.75}$	Table 5	Major-axis diffuse X-ray 75%-flux enclosed radius.	Fig. 6
H_{eff}	Table 6	Minor-axis diffuse X-ray exponential scale height in the 0.3–1.0 keV energy band.	Figs. 6 and 8
$\langle kT \rangle$	Table 8	X-ray emission-integral weighted mean temperature.	Fig. 6
Σ_{HALO}	Table 8	Mean diffuse X-ray surface brightness within the halo spectral extraction region.	Fig. 7
$L_{\text{X,HALO}}$	Table 9	Halo region absorption-corrected X-ray luminosity (0.3–2.0 keV energy band).	Figs. 3 and 4
$L_{\text{X,DISK}}$	Table 9	Disk region absorption-corrected X-ray luminosity (0.3–2.0 keV energy band).	Figs. 3 and 4
$f_{\text{X,HALO}}$	Table 9	Halo region absorption-corrected X-ray flux (0.3–2.0 keV energy band).	Fig. 5

NOTE.—Column 2: Table in this paper, or paper I, in which the symbol in Column 1 is tabulated. Column 3: A short description of the mean of each symbol – see the appropriate Table for a more detailed explanation. Column 4: Figures in this paper in which the values are used. Some data values used in the figures, e.g. $f_{\text{X,HALO}}/\text{fir}$, are not explicitly tabulated but can be calculated from data that is tabulated.

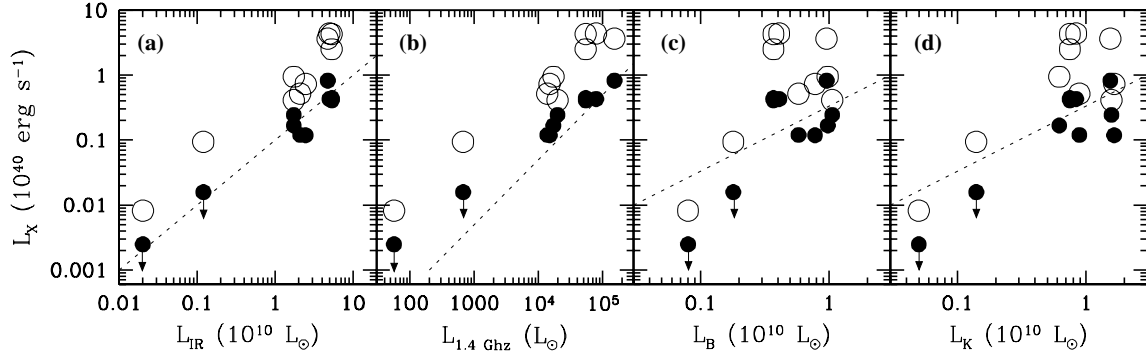


Fig. 3.— Disk and halo diffuse emission 0.3–2.0 keV energy band X-ray luminosities (open and filled circle respectively), plotted against the host galaxies’ total IRAS IR luminosity (panel a), the 1.4 GHz luminosity (panel b), B-band optical luminosity (panel c) and NIR K-band luminosity (panel d). The dotted lines show the trend expected for a relationship of unit slope — they are *not* fits to the data.

4.2. X-ray and multi-wavelength luminosities

We find reasonable correlations between the soft X-ray luminosity of both the disk and halo diffuse X-ray emission, and the total galactic FIR and 1.4 GHz radio luminosities (see Fig. 3), which are well-known measures of the total star-formation rate. In particular, note that the slope of the correlations between L_{IR} or $L_{1.4\text{GHz}}$ and L_X is of order unity, as expected if the diffuse X-ray emission is caused by star-formation activity.

Correlation between the X-ray luminosities and the optical B and NIR K-band luminosities (*i.e.* proxies for total galactic stellar mass) is somewhat weaker, in particular in the case of the halo X-ray luminosity when only detections are considered.

In Fig. 4 we plot all luminosities normalized by the stellar mass of the host galaxy. Estimates of the stellar mass of each galaxy are based on the 2MASS K-band Tully-Fisher relationship derived by Bell & de Jong (2001), and are listed in Table 1. As the K-band luminosity L_K and M_{TF} are not independent variables we have not included a plot of L_X/M_{TF} against L_K/M_{TF} in this figure. Having taken out any dependence related to galaxy mass (*i.e.* more massive galaxies having more star-formation and more X-ray emission than small galaxies), Fig. 4 makes it clear that the diffuse X-ray luminosity per unit mass is directly proportional to star-formation rate per unit mass.

In Fig. 5 we plot the ratio of the absorption-corrected X-ray flux from the halo to the host galaxy’s FIR or radio flux, against estimators of the star-formation rate per unit disk area from radio and FIR

observations, and the galaxy circular velocity. From panels a and b of this figure, it is apparent that all galaxies with detected extra-planar X-ray emission have a similar $f_{X,\text{HALO}}/f_{\text{FIR}}$ ratio, of approximately 4×10^{-5} (± 0.2 dex). The mechanical energy injection rate from supernovae and stellar winds in the starburst is $L_{\text{SN}} \sim 0.01 \epsilon \times L_{\text{FIR}}$, where ϵ is the fraction of mechanical energy thermalized (Heckman et al. 1990). This implies that the halos of these starburst galaxies, along with NGC 891, radiate an approximately fixed fraction $\sim 0.004/\epsilon$ of the mechanical energy supplied by stellar feedback within the disk, in the 0.3–2.0 keV X-ray band. For any realistic value of ϵ , *i.e.* $0.1 \leq \epsilon \leq 1$, we re-derive the well-known result that superwinds radiate a negligible fraction of their energy budget in soft X-rays.

Perhaps the most interesting implication of Fig. 5 is that the X-ray luminosity per unit star formation rate is independent of the star formation intensity (star formation rate per unit disk area), over many orders of magnitude variation in star formation rate per unit area. In other words, the efficiency of converting supernova mechanical power into X-ray emission appears to be independent of the original supernova rate per unit area or volume.

It is also interesting that the normal spiral NGC 891 is so similar to the starbursts in this regard. Fig. 5 also makes it clear that the non-detections of diffuse emission in the halos of NGC 6503 and NGC 4244 are not particularly constraining – given their low FIR and radio brightness we would expect any diffuse X-ray emission generated by star-formation activity to be as

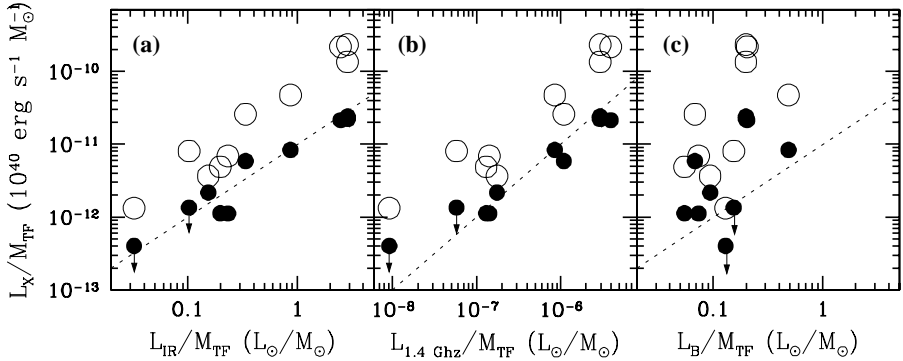


Fig. 4.— As Fig. 3, except all panels are luminosity per unit stellar mass. The disk and halo diffuse emission 0.3–2.0 keV energy band X-ray luminosities divided by total galactic stellar mass are shown and open and filled circles respectively. These values are plotted against IR luminosity per unit mass (panel a), radio luminosity per unit mass (panel b) and B-band optical luminosity per unit mass (panel c). The dotted lines show the trend expected for a relationship of unit slope.

faint or fainter than our existing 3σ limits.

4.3. The size of the X-ray emitting regions

The major-axis X-ray half-light radii $r_{0.5}$ (tabulated in Table 5 of Paper I) provide a convenient measure of the radial size of the diffuse X-ray emission in and near the plane of each galaxy (as a large fraction of the diffuse X-ray emission comes from $z \lesssim 2$ kpc of the plane). To reduce the influence of absorption on the measured sizes we plot $r_{0.5}$ derived from the medium energy band (1.0–2.0 keV) against various simple measures of the radial extent of strong star-formation ($\theta_{1.4\text{GHz}}$), the extent of the old stellar population (D_{25} and the K-band $r_{0.5}$), and the galactic mass (circular velocity v_{rot}) in Fig. 6a – d. The radial extent measure $r_{0.5}$ correlates weakly with $\theta_{1.4\text{GHz}}$, D_{25} and K-band $r_{0.5}$, and not at all with v_{rot} . The 75%-enclosed light radius $r_{0.75}$ shows a somewhat better correlation with D_{25} and the K-band $r_{0.5}$. Quantitatively, the diffuse X-ray radial extent $r_{0.5}$ is closest to the size of the non-thermal radio emission $\theta_{1.4\text{GHz}}$, as expected if the diffuse X-ray emission is generated by mechanical feedback from massive stars. The X-ray emission is more centrally concentrated than the radio emission, although this may be due to the low spatial resolution of the NVSS data.

In contrast, the vertical extent of the diffuse X-ray emission in the halo appears independent of $\theta_{1.4\text{GHz}}$. We have only shown the effective halo exponential scale height H_{eff} in Fig. 6e – h, but the other tracers of

minor axis extent, such as $z_{0.95}$ or z_{1e-9} , produce very similar looking plots. Instead of correlating with local measure of where the energy is injected (such as $\theta_{1.4\text{GHz}}$), the distribution of X-ray-emitting gas at $z \gtrsim 2$ kpc depends on the total size of the host galaxy, given the approximately linear relationship between H_{eff} and D_{25} and/or K-band $r_{0.5}$. More quantitatively, Kendall’s Tau statistic (Press et al. 1992) is only $\tau = 0.21$ for the correlation between $\theta_{1.4\text{GHz}}$ and H_{eff} (1.3σ from zero correlation, equivalently probability of the correlation being spurious $p_s = 0.19$), whereas the stronger correlations mentioned above have $\tau = 0.61$ between D_{25} and H_{eff} (3.8σ , $p_s = 0.00017$), $\tau = 0.43$ between the K-band $r_{0.5}$ and H_{eff} (2.7σ , $p_s = 0.0077$) and $\tau = 0.55$ between v_{rot} and H_{eff} (3.4σ , $p_s = 0.00076$).

Panel j of Fig. 6 plots H_{eff} against the ratio of the mean halo temperature $\langle kT \rangle$ to the mean mass surface density in the disk $\mu = M_{\text{TF}}/D_{25}^2$ (note that the vertical component of the gravitational force g_z is proportional to μ). The correlation not particularly strong, in fact with a $\tau = 0.46$ (2.8σ for zero correlation, $p_s = 0.0045$) it is weaker than the correlations between H_{eff} and D_{25} or v_{rot} . This suggests that the X-ray temperature $\langle kT \rangle$ and scale height H_{eff} are not as directly related as would be the case for simple vertical hydrostatic equilibrium where $H \propto kT/\mu$.

We also investigated the relationship between H_{eff} and the ratio of v_{rot}^2/μ (panel k of Fig. 6). If the vertical support of the gas now visible in X-ray emission was originally due to semi-turbulent gas motions, then

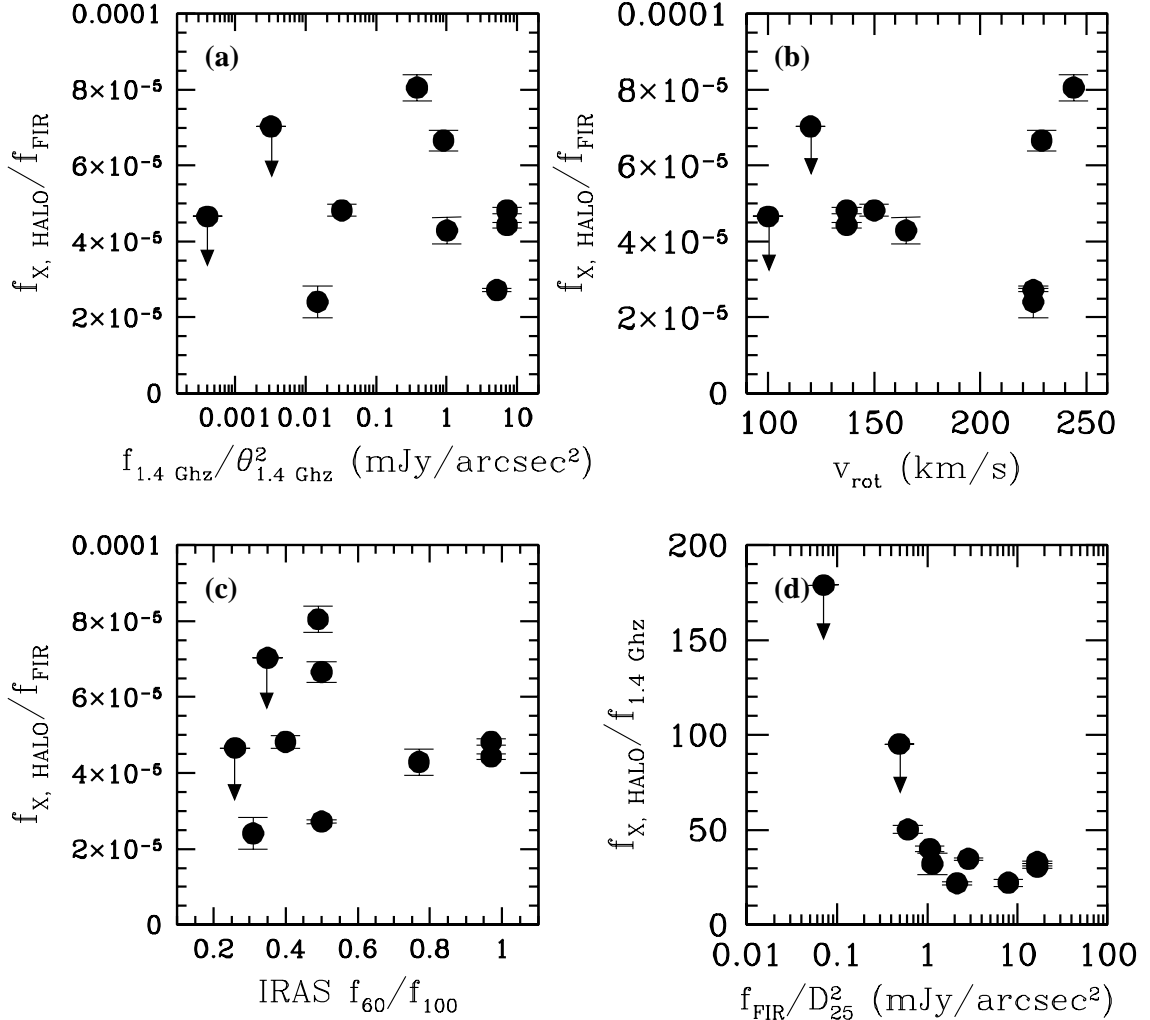


Fig. 5.— Panels a through d plot the ratio of the absorption-corrected 0.3–2.0 keV halo-region X-ray flux to the host galaxies' FIR flux (a, b and c) or 1.4 GHz flux (d) against various proxies for the mean star formation rate per unit area in the host galaxy (panels a, c and d) and galaxy mass (panel b). Error bars show the 1σ statistical errors due to uncertainties in the background-and-point source subtracted count rates alone – systematic uncertainties in $f_{X, \text{HALO}}$ are probably a factor 2 or so. For NGC 6503 and NGC 4244 the 3σ upper limits are shown. For NGC 253 the extrapolated total halo-region flux is used. These results imply that the ratio of the halo X-ray luminosity to the star formation rate of the host galaxy is independent of the concentration or intensity of the star formation, or the mass of the host galaxy.

we might expect the vertical velocity dispersion to be proportional to the rotational velocity of the galaxy (as found for the stellar vertical velocity dispersion, e.g. van der Kruit & de Grijs 1999). Evidence in support of this scenario is lacking in the current data, as the correlation is weak, $\tau = 0.31$ (1.9σ , $p_s = 0.059$).

4.4. The brightness of the diffuse X-ray emission, compared to star-formation intensities and galaxy masses

The presence of correlations between the halo X-ray luminosity and total star-formation rate, and the vertical extent of the X-ray-emitting gas to the total size of the host galaxy, should automatically lead to correlations between the diffuse X-ray surface bright-

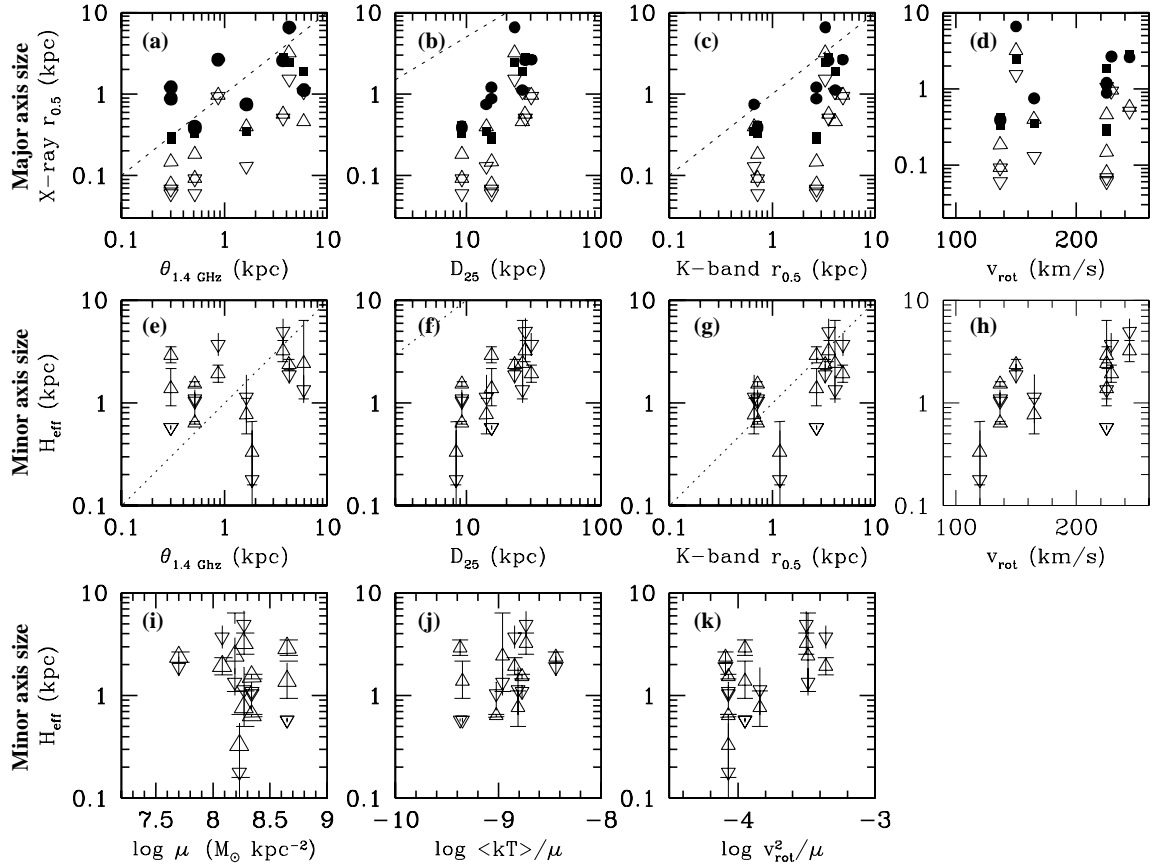


Fig. 6.— A comparison of the characteristic physical dimensions of the diffuse X-ray emission to various proxies for the size of the star-burst region, the optical size of the host galaxy, and galaxy mass (the half-light radius of the 1.4 GHz radio emission $\theta_{1.4\text{GHz}}$, the inclination corrected D_{25} value from the RC3 catalog, the K-band half-light radius from the 2MASS Large Galaxy Atlas (Jarret et al. 2003), and the circular rotation velocity v_{rot}). In panels a to d these values are plotted against the 1.0–2.0 keV energy band major-axis diffuse x-ray half-light and 75%-enclosed light radii $r_{0.5}$ (open symbols) and $r_{0.75}$ (filled symbols), while in panels e through h they are plotted against the minor axis diffuse X-ray exponential scale height H_{eff} in the 0.3–1.0 keV energy band. Data measured along the positive r or z -direction are plotted as open triangles ($r_{0.75}$ values are shown as filled circles), negative r or z as inverted triangles ($r_{0.75}$ values are shown as filled squares). The dotted lines in panels a – c and e – g show the trend an exact one-to-one correspondence between the variables would produce. See discussion in § 4.3. In panels i through k we plot the vertical scale height against the logarithm of mean mass surface density μ (in $M_{\odot} \text{ kpc}^{-2}$), the ratio of the mean X-ray temperature to the mass density (units of keV $\text{kpc}^2 M_{\odot}^{-1}$), and the ratio of the square of the circular velocity to the mass density ($\text{km}^2 \text{ s}^{-2} \text{ kpc}^2 M_{\odot}^{-1}$).

ness and estimates of the star formation rate per unit area (star formation rate intensity, SFRI) in the host galaxy.

This is indeed what we find, as shown in Fig. 7. In panels a through e we plot a variety of proxies for the SFRI, and in panel f the circular velocity, against the mean diffuse X-ray surface brightness within the half-

light height $\Sigma_{0.5}$. Panels g through l repeat this, this time using the halo region surface brightness Σ_{HALO} obtained within the fixed physical-size apertures used in the halo-region spectral fitting.

Although the half light heights are typically only ~ 1 kpc or so, $\Sigma_{0.5}$ is still a measure of the brightness of gas associated with the minor axis outflow in

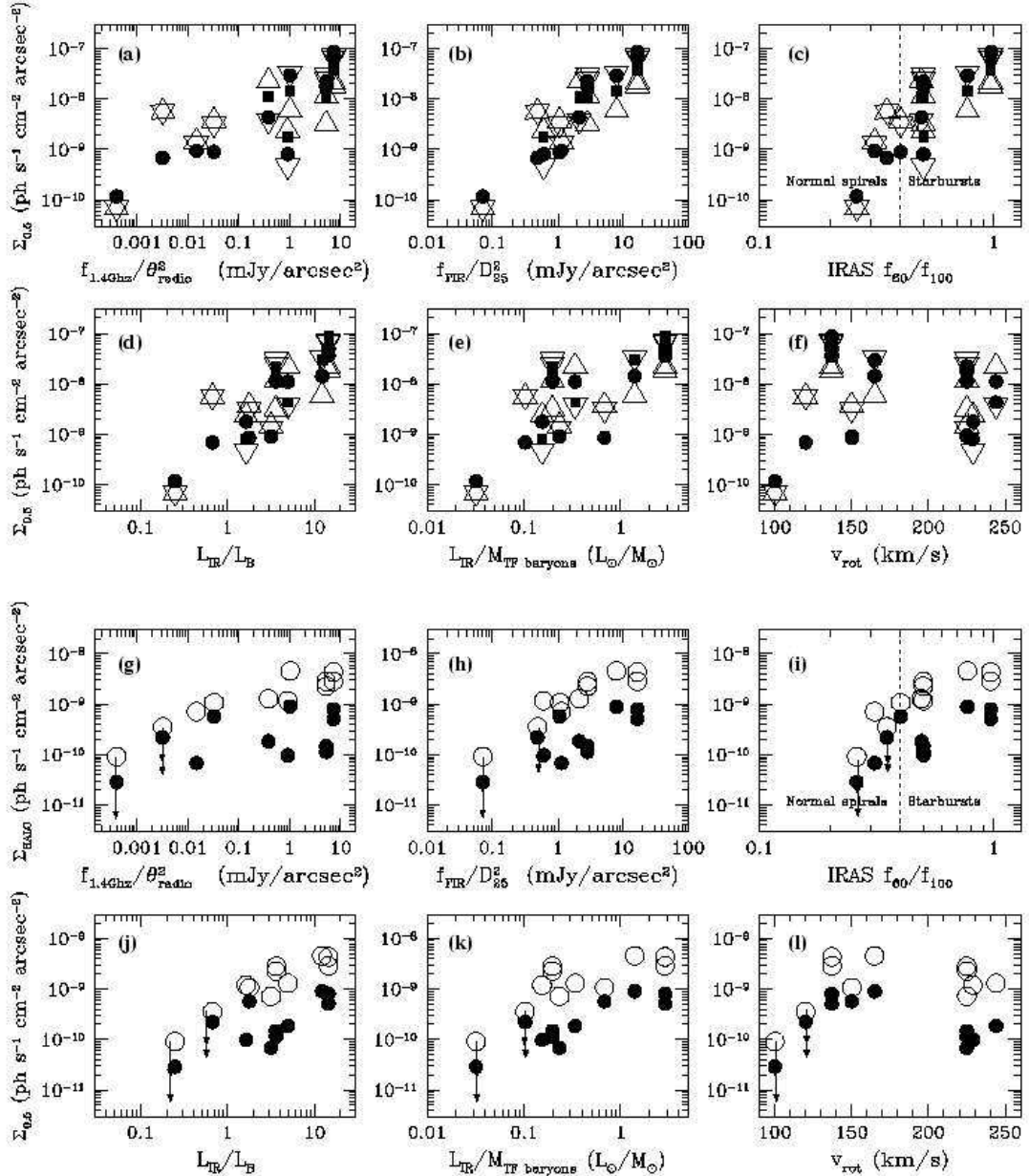


Fig. 7.— Diffuse X-ray surface brightness plotted against various proxies for the intensity of star formation (star formation rate per unit disk area from $f_{1.4\text{GHz}}/\theta_{1.4\text{GHz}}^2$, f_{FIR}/D_{25}^2 or $\log f_{60}/f_{100}$), total star-formation rate per unit galaxy mass (L_{IR}/L_B or somewhat more accurately $L_{\text{IR}}/M_{\text{TF}}$), and galaxy mass (as $M_{\text{TF}} \propto v_{\text{rot}}^{3.51}$). Panels a – f plot the effective X-ray surface brightness $\Sigma_{0.5}$ within the half-light height $z_{0.5}$, which is largely a measure of the brightness near or within the disk. Open symbols correspond to the 0.3–1.0 keV energy band, filled symbols to the 1.0–2.0 keV energy band. Triangles and squares represent data measured along the positive- z direction, inverted triangles and circles data measured along the negative- z direction. Panels g – l plot the mean halo region surface brightness in the 0.3–1.0 keV band (open circles) and the 1.0–2.0 keV band (filled circles). The six-sided stars are cases where values from positive and negative z overlap. See discussion in § 4.4.

the starburst galaxies of this sample. We have demonstrated in this and previous papers that the brightest diffuse X-ray emission is directly associated with optically-emitting gas for which unambiguous kinematic evidence of minor-axis outflow exists (e.g. , in Heckman et al. 1990; McKeith et al. 1995; Shopbell & Bland-Hawthorn 1998). In the normal spirals, NGC 891, NGC 6503 and NGC 4244, there is no existing kinematic evidence for outflow, and hence one might expect $\Sigma_{0.5}$ to trace the brightness of the hot gas *within* the disk (as opposed to lying in projection within 2 kpc of the mid-plane), and also the mean brightness of unresolved point sources.

Note that the correlation between $\Sigma_{0.5}$, or Σ_{HALO} , and the FIR SFRI f_{FIR}/D_{25}^2 (Fig. 7b and h, where the angular size D_{25}^2 is that of the old stellar population, and hence independent of the angular size of the main star forming region in the host galaxy) are better than the correlations between $\Sigma_{0.5}$ or Σ_{HALO} and the NVSS 1.4 GHz SFRI $f_{1.4\text{GHz}}/\theta_{1.4\text{GHz}}^2$ (Fig. 7a and g, where $\theta_{1.4\text{GHz}}$ is a direct, although low spatial resolution, measure of the size of regions in which SNe are occurring). This is due to the better correlation between the vertical extent of the extra-planar emission with the total size of the host galaxy, than with the radial size of the main star-formation regions.

The ordinate values in panels d, e, j and k of Fig. 7 are, to first order, star formation rate per unit galactic mass. These panels, along with panels f and l (which plot $\Sigma_{0.5}$ and Σ_{HALO} against the circular velocity v_{rot}), show that the brightness of the diffuse X-ray emission does not correlate with galactic mass, and hence is genuinely *caused* by star formation. It is therefore not the case that the correlation in panels a through c, and g through h, is spurious and arises simply because more massive galaxies, which can hold more hot gas in their potential wells, also have more star-formation in total.

Again, it is intriguing that there is no obvious transition in X-ray surface brightness between the normal and starbursting spirals – the normal spirals follow the trends one could extrapolate on the basis of the starburst galaxies alone.

In summary, these results validate the basic assumption that the presence of extra-planar diffuse X-ray emission is driven by star-formation processes in the underlying disk, but that the large-scale structure of the host galaxy also plays a strong role in determining the properties of the extra-planar emission.

In Fig. 8 we show the observed vertical extent of the diffuse X-ray emission against estimates of the SFRI (recast in terms of supernova rate per unit area F_{SN}) and total galactic mass M_{TF} for the galaxies of our sample. We estimate the supernova rate based on the IRAS FIR flux. Dividing this SN rate by the inclination corrected D_{25}^i value gives $F_{\text{SN,FIR},D_{25}}$, the mean SN rate per unit area of the entire disk. If instead we use the approximate diameter of the non-thermal radio emission $\theta_{1.4}$ we obtain $F_{\text{SN,FIR},\theta_{1.4\text{GHz}}}$ (See Tables 1 and 2 for the origin of these values). It is clear that *there is no correlation between the vertical extent of the diffuse X-ray emission and the SN rate per unit area in the host galaxy*, except that galaxies with lower SN rate per unit area than NGC 891 have no detected extra-planar X-ray emission. This is similar to the finding by Dahlem et al. (2001), who found no correlation between the vertical scale height of non-thermal radio emission and the star formation rate per unit area in a sample of edge-on disk galaxies.

Fig. 6, in combination with Fig. 8, implies that the density scale height of the X-ray emitting material depends on the absolute size of the host galaxy, and not on the spatial distribution or intensity of star formation within it. Note that this is not a statement regarding the absolute physical extent of superwinds, which almost certainly is much greater than the region probed by current observations (and which will physically depend on the total amount of energy deposited by SNe and the density of the IGM).

We were initially motivated to investigate the quantitative relationship between the extra-planar X-ray properties and the SFRI indicators L_{FIR}/D_{25}^2 and $f_{1.4\text{GHz}}/\theta_{1.4\text{GHz}}^2$ by optical studies of the eDIG (see Dettmar 1992; Rand 1996; Hoopes et al. 1999, among others). These had demonstrated the presence of extra-planar optical emission correlated with L_{FIR}/D_{25}^2 , in the sense that galaxies with high values of L_{FIR}/D_{25}^2 were more likely to show evidence of eDIG. Combined with the studies of Lehnert & Heckman (1995, 1996); Dahlem et al. (2001) that demonstrate that IR-warm galaxies with $f_{60}/f_{100} > 0.4$ are extremely likely to have extra-planar emission, kinematic evidence of outflow and/or non-thermal radio halos, we expected a correlation between high star formation rate per unit area and the luminosity and extent of diffuse X-ray emission in disk galaxy halos.

Nevertheless, in the X-ray band it appears that the correlation we have found between the surface brightness of the diffuse X-ray emission and star formation

rate per unit area is the combination of two independent effects:

1. A relatively uniform efficiency of converting mechanical energy to X-ray emission (§ 4.2), *i.e.* $f_X \propto f_{\text{FIR}}$, the exact physics of which is not fully understood.
2. The vertical extent of the X-ray emission is directly related to the size of the host galaxy, $H_{\text{eff}} \propto D_{25}$ (§ 4.3), possibly for the reasons discussed below.

This does not mean that the SFRI is not an important parameter, in particular when considering the conditions necessary to drive gas into the halo of a galaxy (as we shall discuss below), but that other parameters play a significant role in shaping the emission we see.

In terms of the interpretation of the extra-planar X-ray and H α emission presented in Paper I (and summarized in § 3), item 2 above can be explained if disk galaxies have gas throughout their halos, with vertical density scale heights approximately similar to the optical diameter of the host galaxy. Depending on the exact model assumed the mass of gas in the halo of a Milky Way-like galaxy *prior* to any starburst is a few times 10^7 to a few times $10^8 M_{\odot}$ (see models 4 and 5 in Strickland et al. 2002a).

4.5. Limits placed on cosmological accretion models for the origin of hot gas in the halos of normal galaxies

Without deep X-ray observations of a larger sample of edge-on normal spiral galaxies it is difficult to critically test cosmological accretion models of the type presented by Toft et al. (2002), and Sommer-Larsen et al. (2002). Excluding the starbursts from consideration for the time being being, we would expect halo 0.3–2.0 keV X-ray luminosities of order $L_X = 4.60, 0.20$ and $0.08 \times 10^{38} \text{ erg s}^{-1}$ for NGC 891, NGC 6503 and NGC 4244 respectively, based on the Toft et al. model.

Here we have assumed the X-ray emission has a fixed temperature of 0.17 keV (the emission-integral-weighted mean temperature obtained for NGC 891⁷), a metal abundance $Z = 0.3 Z_{\odot}$ (the result is largely independent of Z), and is described by an exponential surface brightness profile with a fixed surface brightness

scale height of 2 kpc (as Toft et al. 2002 do not provide any measure of how the characteristic size of the X-ray emission varies with galaxy rotation velocity). For such a distribution a fraction e^{-1} of the total luminosity arises in gas at $|z| \geq 2$ kpc. Toft et al. (2002)'s predicted bolometric luminosity (0.012–12.4 keV energy band) of $L_{\text{BOL}} \sim 10^{40} (v_{\text{rot}}/230 \text{ km s}^{-1})^5 \text{ erg s}^{-1}$ (scatter ± 0.5 dex) thus converts to a total 0.3–2.0 keV X-ray luminosity (*i.e.* integrated over all heights z) of $L_X \sim 1.4 \times 10^{39} (v_{\text{rot}}/230 \text{ km s}^{-1})^5 \text{ erg s}^{-1}$ (for simplicity we ignore the fact that the halo temperature should vary with rotation velocity as approximately $kT \propto v_{\text{rot}}^2$, as hence even lower X-ray fluxes would be expected in the 0.3–2.0 keV energy band for NGC 6503 and NGC 4244).

The predicted accreted halo luminosities given in the first paragraph of this section should be compared to the observed values of $L_{X,\text{HALO}} = 1.2 \times 10^{39} \text{ erg s}^{-1}$ for N891 and 3σ upper limits of $L_{X,\text{HALO}} < 1.6 \times 10^{38} \text{ erg s}^{-1}$ and $< 2.5 \times 10^{37} \text{ erg s}^{-1}$ for NGC 6503 and NGC 4244 respectively (see Table 9 of Paper I). This comparison indicates that the predicted accretion-model X-ray luminosity for a galaxy like NGC 891 is close to that value observed, and that the NGC 4244 and NGC 6503 observations are not deep enough to strongly constrain the accretion model. Although, based on luminosity alone, some fraction of the X-ray emission in the halo of NGC 891 might be due to gas accreted from the IGM, we find the reasoning presented in § 4.2, 4.3 and 4.4 more compelling as evidence that the extra-planar X-ray emission in NGC 891 is associated with, and dominated by, feedback from star-formation.

This apparent commonality of normal spirals with starbursts, based on the properties of their extra-planar emission, might be an artifact of the small number statistics. Deep X-ray observations of other edge-on normal spirals, spanning a broad range of star-formation rates, are clearly necessary before firmer conclusions can be drawn. Nevertheless, a robust finding of a smooth transition in the halo gas properties from normal to starburst galaxies would have major implications for understanding the large-scale structure of the ISM and stellar feedback processes in galaxies.

⁷The virial temperature for NGC 891 is $kT_{\text{vir}} = \mu m_{\text{H}} v_{\text{rot}}^2 = 0.16 \text{ keV}$. This may be a coincidence, since for the starburst galaxies $\langle kT \rangle$ shows no correlation with v_{rot} .

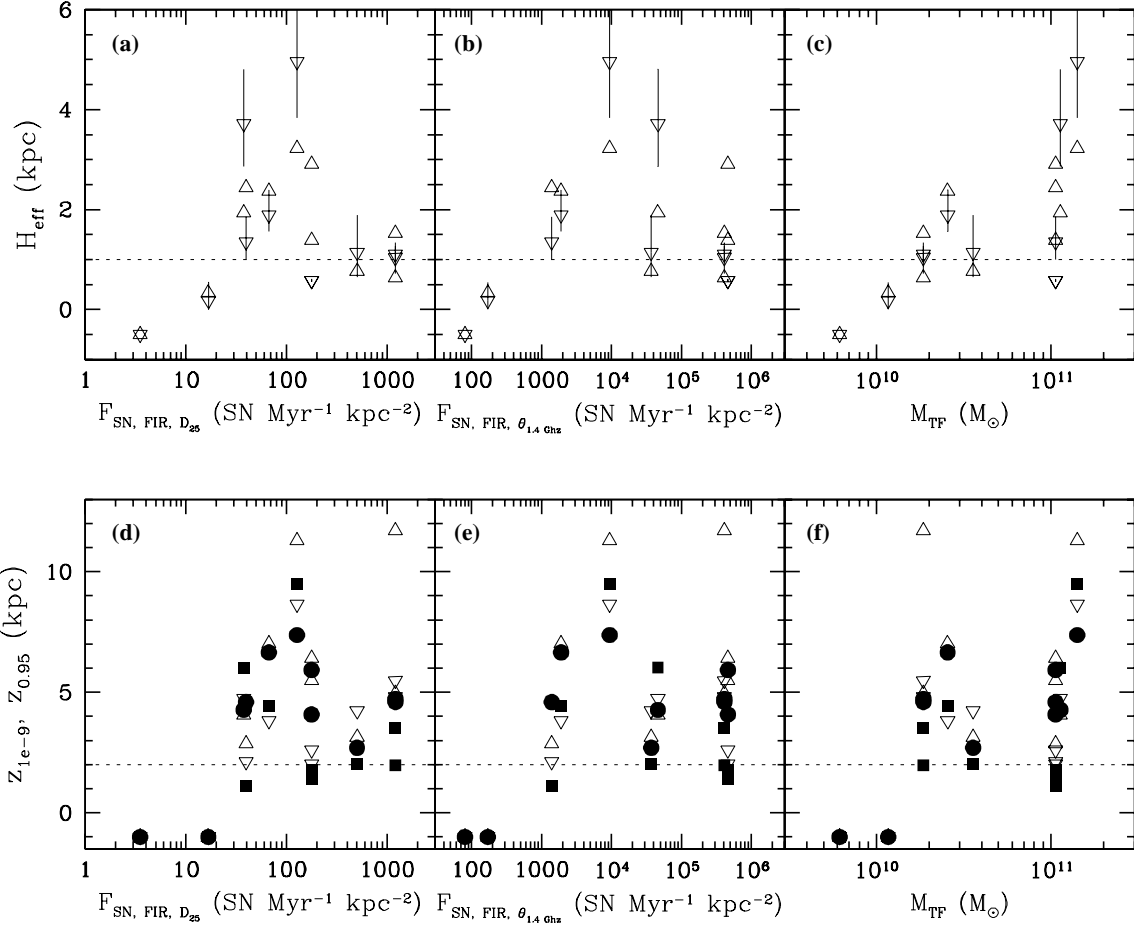


Fig. 8.— The vertical extent of the diffuse X-ray emission as a function of the mean SN rate per unit area F_{SN} or circular velocity v_{rot} of each galaxy. See § 5.1.2 for a description of how $F_{\text{SN,FIR,} D_{25}}$ and $F_{\text{SN,FIR,} \theta_{1.4 \text{ GHz}}}$ were calculated. Panels a – c plot the fitted surface brightness scale height for $z \geq 2$ kpc, data from positive z shown as open triangles and negative z as inverted triangles. The horizontal dashed line corresponds to a gas density scale height of 2 kpc. Panels d – g plot the isophotal minor axis size z_{1e-9} (positive z data points shown as open triangles, negative z as filled circles) and 95% enclosed minor axis light height $z_{0.95}$ (positive z data points shown as filled circles, negative z as filled squares). Where no measurement can be made a negative value is shown.

5. Comparison the theoretical models of mechanical energy feedback from massive stars

5.1. Disk blow-out energy requirements

In a seminal paper, Mac Low & McCray (1988) considered, both analytically and numerically, the amount of mechanical energy that supernovae and stellar winds need to supply for a superbubble to blow-out of the stratified atmosphere of a galactic disk. This theory, with minor alterations, has been widely used since that time, in particular with respect to assessing

the prospects for metal ejection from galaxies (e.g. Koo & McKee 1992; Martin 1996; Mac Low 1996; Tenorio-Tagle 1996; Silich & Tenorio-Tagle 1998; Mac Low & Ferrara 1999; Ferrara & Tolstoy 2000; Ferrara, Pettini & Shchekinov 2000; Silich & Tenorio-Tagle 2001).

For such an important theoretical construct, there has been surprisingly little in the way of observational testing and calibration. Heckman et al. (1990) demonstrated that the energy injection rates in starburst galaxies exceeded this critical blow-out luminos-

ity (hereafter L_{CRIT}), but is is not clear from that work (and other comparisons to starbursting galaxies e.g. Martin 1996) what the lowest energy injection rate is that leads to blow-out in real galaxies.

In this section we shall use the observationally determined presence of hot gas in the halos of our sample galaxies as empirical evidence for blow-out from the disk, and compare the estimated rates of SN energy return in disks of these galaxies to theoretical values of L_{CRIT} .

5.1.1. The critical mechanical luminosity for disk blow-out

The theoretical critical mechanical luminosity required for blow-out is based on the following concepts. If, in a stratified disk with a vertical gas density distribution $\rho_z = \rho_0 \exp(-z/H)$, an expanding superbubble or SN remnant has an expansion velocity v_{bub} greater than the sound speed $c_s = (\gamma P/\rho)^{1/2}$ in the ambient ISM by the time it reaches a vertical height of order the scale height H of the disk, then the shock wave will begin to accelerate. At this time the bubble or remnant shell will fragment due to Rayleigh-Taylor instabilities. The hot, high pressure, plasma interior to the shell will vent out through the fragmented shell into the halo. If $v_{\text{bub}} \lesssim c_s$, the bubble's expansion will continue to decelerate and eventually coast to a stop without blowing out. Radiative cooling will eventually lead to depressurization of the bubble interior, followed by the collapse of the bubble, in addition to damage caused by galactic differential rotation and random ISM motions. A more formal analysis identifies $v_{\text{bub}} > c_s$ at $z = 3H$ as the critical requirement for blow-out in a single-phase exponential atmosphere (see Ferrara & Tolstoy 2000), numerically verified by simulations showing blowout occurring once the bubble reaches a height of $\sim 3H$ (Mac Low & McCray 1988; Mac Low, McCray & Norman 1989)

For a bubble driven by a constant mechanical luminosity L_W into a medium of uniform and constant ambient density ρ_0 (Castor, McCray & Weaver 1975; Weaver et al. 1977), the radius r_{bub} and shell expansion velocity v_{bub} as a function of time t are

$$r_{\text{bub}} = \alpha L_W^{1/5} \rho_0^{-1/5} t^{3/5}, \quad (1)$$

and

$$v_{\text{bub}} = 0.6 \alpha L_W^{1/5} \rho_0^{-1/5} t^{-2/5}, \quad (2)$$

where $\alpha = (125/154\pi)^{1/5}$. Rearranging these equations gives us the expansion velocity at the point that

the bubble radius is $3H$:

$$v_{3H} = 0.6 \times 3^{-2/3} \mathcal{F}_v \alpha^{5/3} L_W^{1/3} \rho_0^{-1/3} H^{-2/3}, \quad (3)$$

where \mathcal{F}_v is a numerically-determined correction factor to account for the vertical decrease in density leading to bubble expansion velocities greater than in the constant density case. Using a code that numerically integrates the appropriate equations of motion (Strickland & Stevens 1999), we find $\mathcal{F}_v = 2.5^8$.

The resulting minimum mechanical luminosity required to blow out of this atmosphere, L_{CRIT} , is

$$L_{\text{CRIT}} = (154\pi/3) \gamma^{3/2} \mathcal{F}_v^{-3} \rho_0^{-1/2} P_0^{3/2} H^2, \quad (4)$$

where P_0 is the thermal pressure in the ambient ISM. Note that this luminosity is a factor ~ 3 lower than the critical luminosity derived by Mac Low & McCray (1988), *i.e.* blow-out from the disk is slightly easier. Converting to units more appropriate for the disk of a normal spiral,

$$\frac{L_{\text{CRIT}}}{10^{38} \text{ erg s}^{-1}} = 3.43 n_0^{-1/2} \left(\frac{P_0}{10^4 k} \right)^{3/2} \left(\frac{H}{1 \text{ kpc}} \right)^2, \quad (5)$$

where $n_0 = \rho_0/\mu m_H$ and $\mu m_H = 10^{-24} \text{ g cm}^{-3}$. More energy is needed to blow out of a starburst region, where measured ISM pressures reach $P/k \gtrsim 10^7 \text{ K cm}^{-3}$ (Heckman et al. 1990).

Energy return from non-interacting star clusters

If one assumes that a superbubble can only be powered by a single OB association, then only the most massive OB associations will be able to create superbubbles capable of blowing out of a disk galaxy. The critical energy given in Eqn. 5 corresponds to the energy returned from all of the core-collapse SNe events in a cluster of mass $2.3 \times 10^4 \epsilon^{-1} M_\odot$ (equivalently $\sim 190 \epsilon^{-1}$ SNe over ~ 40 Myr), assuming a Salpeter IMF between lower and upper stellar mass limits of 1 and $100 M_\odot$ respectively. The thermalization efficiency ϵ is the fraction of the initial 10^{51} erg of initial kinetic energy per supernova that can be used to drive the bubble, *i.e.* the energy fraction not radiated away prior to each young remnant overlapping with other SN remnants.

⁸Ferrara & Tolstoy (2000) present a purely analytical derivation of v_{3H} including the effect of the density decline, but we find this method over-predicts v_{3H} by a factor 3.7 over our numerical result (even when errors in their equations 24 and 25 are corrected for). We speculate that this discrepancy is due to their neglect of the inertia of the cold shell in their calculation of the shock velocity.

Ferrara et al. (2000) consider metal ejection into the IGM in such a model. Through Monte Carlo modeling considering the observed luminosity function of OB associations, they show that it is rare to find an OB association that will yield more than ~ 400 SNe, which is very close to the critical value required for blow-out from the disk of a normal spiral. Hence only a very small fraction of SN events lead to blow-out.

For readers skeptical of purely theoretical arguments, consider the masses of the most spectacular and massive star clusters in the Local Group. The Arches cluster in the Galactic center, although containing $\sim 5\%$ of all the Wolf-Rayet stars in the Galaxy, has a mass $< 7 \times 10^4 M_\odot$ (Figer et al. 2002). The R136 cluster in the 30 Doradus nebula of the LMC has an estimated initial mass of $\gtrsim 1.7 \times 10^4 M_\odot$ (Malamuth & Heap 1994), or $\sim 3 \times 10^4 M_\odot$, upper limit $1.5 \times 10^5 M_\odot$ (Brandl et al. 1996).

A more typical OB association, the Orion Nebula Cluster, has a total gravitating mass of $4.5 \times 10^3 M_\odot$ (Hillenbrand & Hartmann 1998). A canonical value of the supernova thermalization efficiency under normal interstellar conditions is $\epsilon = 0.1$ (Thornton et al. 1998, note that ϵ is expected to be higher in regions of higher star formation rate per unit volume, e.g. Larson 1974). The Milky Way has a gaseous scale height of ~ 0.5 kpc in the neutral ISM (Sembach & Danks 1994), and between $0.5 - 1.5$ kpc for the free electrons tracing the warm ionized component (Reynolds 1989; Nordgren, Cordes & Terzian 1992). Taking these values together, it is clear that it is impossible for an OB association similar to the Orion Nebula Cluster to create, on its own, a bubble capable of breaking out of the disk (if the theory presented above is correct).

Single OB association blow-outs, even from the most massive individual clusters, are unlikely to account for the extra-planar diffuse X-ray we observe around a normal galaxy such as NGC 891. Given that L_X will be at most a few percent of the total energy injection rate L_W (see § 5.1.2), individual bubbles provide too little X-ray luminosity. Clearly, the base assumption of non-interacting clusters is unsatisfactory.

Collective energy return over galactic scales

In reality, star clusters tend themselves to cluster spatially, with starbursts representing the extreme of the phenomenon (one can describe the M82 starburst as ~ 100 R136's within a region only 2–3 times larger than 30 Doradus, see O'Connell et al. 1995). Fur-

thermore, Meurer et al. (1995) demonstrate that only a fraction $\sim 20\%$ of the massive stars within nearby starburst regions are associated with clusters, there being a substantial “field” population of massive stars (see also Tremonti et al. 2001; Chandar et al. 2003).

Inspired by this, we adopt a position at the opposite extreme from that adopted by Ferrara et al. (2000). Mac Low & McCray (1988) find that at blowout the radius of the superbubble within the disk is $\sim H$. We therefore assume that some significant fraction Υ of all SNe due to massive star formation within an area πH^2 of the disk can contribute energetically to creating a blowout, *i.e.* .

$$L_W = \pi H^2 F_{SN} \epsilon \Upsilon E_{SN}, \quad (6)$$

where F_{SN} is the SN rate per unit disk area, and $E_{SN} = 10^{51}$ erg is the kinetic energy return per SN event. Combining this with Eqn. 4, we obtain the critical SN per unit disk area for blow out, $F_{SN,CRIT}$, to be

$$F_{SN,CRIT} = (154/3) \gamma^{3/2} \mathcal{F}_v^{-3} \rho_0^{-1/2} P_0^{3/2} (\epsilon \Upsilon E_{SN})^{-1}. \quad (7)$$

Note that this is no longer dependent on the scale height. Large gaseous scale heights do not inhibit blow out as the bubble can draw mechanical energy from a correspondingly larger region of disk. Scaling to more convenient units,

$$F_{SN,CRIT}(\text{Myr}^{-1} \text{kpc}^{-2}) = 3.45 \times n_0^{-1/2} \left(\frac{P_0}{10^4 k} \right)^{3/2} \left(\frac{1}{\epsilon \Upsilon} \right), \quad (8)$$

or alternatively

$$F_{SN,CRIT}(\text{Myr}^{-1} \text{kpc}^{-2}) = 3.45 \times \left(\frac{P_0}{10^4 k} \right) \left(\frac{1}{\epsilon \Upsilon} \right) \left(\frac{T_0}{10^4} \right)^{1/2}. \quad (9)$$

Theoretically, both ϵ and Υ are functions of the star formation rate, as supernovae alter the porosity of the ISM, and hence alter radiative energy losses and the effectiveness of collective action (Larson 1974).

Ideally, F_{SN} should be calculated on a location-by-location basis within a given galaxy, based on the local supernova rate \mathcal{R}_{SN} , or star formation rate, summed within an area πH^2 , where H is the appropriate gas density scale height for the region we are interested in assessing blow out from (be it the thin molecular disk, the more extended Reynolds layer, or the halo itself) — *i.e.* some knowledge of the scale height is still required.

5.1.2. Constraining feedback efficiencies through comparison to observations

Given that we have demonstrated that the origin of the diffuse emission is due to SN feedback, assessing whether significant blow out has occurred reduces to the simple matter of identifying which galaxies have diffuse X-ray emission at $z \gtrsim 2$ kpc. With the addition of accurate values of the SN rate per unit area for each galaxy we can then measure a lower limit to $\epsilon\Upsilon$ (assuming the blow out theory is correct), or given independently determined values of $\epsilon\Upsilon$ directly test the blow out theory.

Given the large uncertainties in some of the observational parameters, in particular the star formation and SN rates per unit area, what follows is intended more as a demonstration of the method than the final word on the subject.

Constraints on feedback efficiencies from the observed luminosities

We can crudely constrain the mechanical energy feedback efficiency by relating the rate of mechanical energy injection into the halo to the observed X-ray luminosities.

From the relationship between the FIR luminosity and SN rate given in Heckman et al. (1990), $R_{\text{SN}} = 0.2L_{\text{FIR}}/10^{11} L_{\odot}$, we obtain that the rate of mechanical energy injection into the halo is

$$L_{\text{W,HALO}} = 0.0167 \epsilon\Upsilon L_{\text{FIR}}. \quad (10)$$

Direct observation of the volume-filling high-pressure gas that drive superwinds would be the best method of measuring the supernova thermalization efficiency. In the absence of this we are forced to estimate ϵ from a theoretically-determined relationship between the X-ray luminosity and the mechanical power actually driving the wind. The fraction $A_{\text{XRAD}} = L_{\text{X,HALO}}/L_{\text{W,HALO}}$ depends on the physical process responsible for the soft X-ray emission, e.g. non-radiative wind shocks, or possibly conductive interfaces between hot and cold gas. For X-ray emission from conductive interfaces (Weaver et al. 1977; Chu & Mac Low 1990), which is the mechanism that has been most extensively explored to date, A_{XRAD} depending only weakly on the ambient density and value of thermal conductivity (L_{X} scales almost exactly in proportion to L_{W} , and increases weakly for higher ambient density or thermal conductivity). We calculated

A_{XRAD} for conditions appropriate for superwinds using the code described in Strickland & Stevens (1999), which numerically solves the Weaver et al. (1977) model and uses the Mewe et al. (1995) hot plasma code to calculate the X-ray emission. For $L_{\text{W,HALO}}$ in the range 10^{40} to 10^{42} erg s $^{-1}$, gas densities in the range 10^{-3} to 1 cm $^{-3}$, ages in the range 5 to 30 Myr and values of the thermal conductivity in units of the Spitzer conductivity 0.1 to 10, we find a mean $A_{\text{XRAD}} = 0.013$ (with a scatter ± 0.6 dex). In our hydrodynamical simulations of superwinds (Strickland & Stevens 2000), which do not include thermal conduction, we find a similar fraction of the mechanical energy emerging in the soft X-ray band (again with a significant scatter, depending on the exact initial conditions assumed).

For the time being we shall assume that $A_{\text{XRAD}} \sim 0.01$ is a reasonable estimate of the fraction of the wind mechanical power that is radiated in the soft X-ray band. Combining this with Equation 10 we obtain

$$L_{\text{X,HALO}} \sim 1.67 \times 10^{-4} (A_{\text{XRAD}}/0.01) \epsilon\Upsilon L_{\text{FIR}}. \quad (11)$$

The typical $f_{\text{X,HALO}}/f_{\text{FIR}}$ ratio we observe is $\sim 4 \times 10^{-5}$, which implies thus $\epsilon\Upsilon \sim 0.24$. NGC 891 has one of the lowest $f_{\text{X,HALO}}/f_{\text{FIR}}$ ratios of the sample of 2.22×10^{-5} (NGC 891 is the lowest if we exclude the somewhat doubtful detection of halo emission from NGC 4945), and thus a lower than average value for $\epsilon\Upsilon \sim 0.14$.

Testing blow-out theory

Currently we only have a crude estimate of the total supernova rate \mathcal{R}_{SN} of each of these galaxies⁹, which prevents us from calculating F_{SN} in the manner described in § 5.1.1. Nor do we have exact measures of the scale height of the disk ISM. However, considering the issue of disk blow out, this scale height is likely to be of order a few hundred parsecs to a kiloparsec or two. As this is similar to the magnitude

⁹We note that H α imaging could be used to evaluate F_{SN} on a location-by-location basis within the same galaxy, although this method has typically been used to calculate mean galactic SFRI values and blow-out thresholds (e.g. Rossa & Dettmar 2003). H α emission in the disk is typically much more radially extended than the regions responsible for driving the outflow (the exception being M82, where star-formation is now confined solely to the nuclear region), *i.e.* star formation in some regions of the disk is occurring at rates per unit area below the critical value. This is graphically illustrated in Fig. 1 and 2. Of course, H α measurements suffer the weakness that they systematically underestimate the true SFRI in the regions with the highest star formation rates due to the associated higher levels of extinction.

of $\theta_{1.4\text{GHz}}$ (see Table 2), it is not unreasonable to use $\mathcal{R}_{\text{SN}}/(4\theta_{1.4\text{GHz}}^2)$ as an approximation to the appropriate F_{SN} to use when assessing disk blow out (this value is denoted as $F_{\text{SN},\text{FIR},\theta_{1.4\text{GHz}}}$ in Table 2 and in Fig. 8).

In Fig. 8b and e we show the observed vertical extent of the diffuse X-ray emission against $F_{\text{SN},\text{FIR},\theta_{1.4\text{GHz}}}$. The strongest test of disk blow out theory is given by the lowest observed F_{SN} value unambiguously associated with disk blow out. From Fig. 8 it appears that all galaxies with $F_{\text{SN},\text{FIR},\theta_{1.4\text{GHz}}} \gtrsim 1400 \text{ SN Myr}^{-1} \text{ kpc}^{-2}$ have diffuse extra-planar X-ray emission, indicative of disk blow out. Let us assume that the divide between disk blow out and superbubble confinement occurs at or near this value of F_{SN} . As the galaxy with the lowest F_{SN} value that also has *detected* extra-planar emission is the normal spiral galaxy NGC 891, let us assume that $n_0 \sim 1 \text{ cm}^{-3}$, $P/k \sim 10^4 \text{ K cm}^{-3}$ and $\epsilon\Upsilon \sim 0.14$. Thus equation 8 would then predict disk blow out for $F_{\text{SN}} \gtrsim 25 \text{ SN Myr}^{-1} \text{ kpc}^{-2}$, a factor ~ 50 lower than the observationally-estimated value.

One possible interpretation is that disk blow out is considerably more difficult than simple analytical and numerical theory predicts.

Alternatively, we may have over-estimated $\epsilon\Upsilon$ for NGC 891, if a larger fraction of the mechanical energy reaching the halo can be radiated in the soft X-ray band. Furthermore, galaxies with lower F_{SN} may well drive hot gas into their halos — the limits placed on halo X-ray emission by the observation of the intrinsically faint normal galaxies NGC 6503 and NGC 4244 do not sufficiently constrain the problem. If either of these scenarios is true then the standard theory may be correct.

Within a few years, deep observations with *Chandra* and *XMM-Newton* of edge-on normal star forming galaxies should be able to place much tighter constraints on the F_{SN} at which blow out from the disk occurs. A better understanding of the emission processes in superwinds (and whether they apply to fountain-like flows) is also necessary before we can confidently evaluate A_{XRAD} and $\epsilon\Upsilon$. Moderate-to-high spatial resolution IR observations with *SIRTF* will allow the star formation rate to be measured as a function of position within these galaxies. This is important for obtaining accurate values of F_{SN} in the more normal disk galaxies, where different regions of the star-forming disk may lie on either side of the critical F_{SN} for disk blow out. Although currently somewhat limited by the quality of existing theoretical and observation data, this method has the potential to allow stringent tests of this

currently poorly-tested but cosmologically-important theory of superbubble blow-out.

5.2. Ejection of metal-enriched gas

5.2.1. The plausibility of halo blow-out

Material blowing out from the disk does not automatically escape into the IGM, as it must work against the obstacle provided by gas in the halo before being able to reach the IGM, as mentioned in § 1.

Based on the observed X-ray surface brightness profiles of the extra-planar emission of the galaxies within this sample, it is appropriate to represent the original halo gas distribution as an exponential with density scale height $H_g \sim 4 - 8 \text{ kpc}$, *i.e.* twice the observed surface brightness scale height.

The standard blow out energy requirement then applies, this time with respect to halo blow out, to any bubble or wind that manages to blow out of the disk. Note that this directly implies that the critical region of space around a galaxy that can prevent escape into the IGM is within $\sim 3H_g$ ($\sim 12 - 24 \text{ kpc}$) of the mid-plane, a region that can be probed by existing observational methods. We need not concern ourselves about the density and pressure of gas at larger, $\sim 100 \text{ kpc}$, distances from the host galaxy¹⁰.

We can now apply the arguments of § 5.1 to halo blow out. The proportionality between the halo region X-ray flux and the IRAS FIR flux (and hence the *total* galactic SF rate) strongly suggests that the halo can draw on mechanical energy from a significant fraction of the entire star-forming disk. If the SN rate per unit area in the disk is sufficient to blow out from the disk, then the collective blow-out model can be applied to the halo. The appropriate scale height to use is that of the halo gas density distribution H_g . Conveniently, it appears from the empirical results of § 4.3 that $H_g \propto D_{25}$ (or the K-band half light radius $r_{0.5}$). Thus the appropriate F_{SN} to calculate for assessing halo blow out is proportional to $\mathcal{R}_{\text{SN}}/D_{25}^2 \equiv F_{\text{SN},\text{FIR},D_{25}}$.

The only significant differences from the case of assessing disk blow out are then as follows:

1. The appropriate density and pressure are that of the halo, evaluated at the galactic midplane (e.g.

¹⁰This is true unless the galaxy happens to be in a high density environment such as a cluster or compact group, where the pressure and density of the inter-cluster or inter-group medium may be significant, in which case the arguments of Silich & Tenorio-Tagle (1998); Murakami & Babul (1999); Silich & Tenorio-Tagle (2001) apply.

see Shull & Slavin 1994). For typical galactic environments now and at high redshift, the density and pressure of any bound, non-transient, halo medium will be less than those in disk.

2. The additional energy losses during disk blow must be accounted for. In the starbursts, a good case can be made that radiative losses are negligible, based both on the observational lack of significant X-ray, O VI and optical emission (Heckman et al. 1990, 2001; Hoopes et al. 2003). In the high resolution hydrodynamical simulation of Strickland & Stevens (2000) $\gtrsim 50\%$ of the mechanical energy injected within the disk is transported into the halo.

3. When considering blow out from the halo it is appropriate to use a SN rate averaged over the characteristic size of the host galaxy, not just the main star forming region. For comparison to Eqn. 7 a good estimate of F_{SN} would be $\mathcal{R}_{\text{SN}}/(\pi H_{\text{g}}^2) \approx \mathcal{R}_{\text{SN}}/(4\pi r_{0.5, \text{K-band}}^2)$ or $\mathcal{R}_{\text{SN}}/(0.04\pi D_{25}^2)$, given the correlations shown in Fig. 6.

Making full use of this to assess blow out from the halos of galaxies requires that we know the critical SN rate per unit area for disk blow out. Nevertheless, with an observationally-calibrated theory of this sort it will be possible to assess whether gas can blow out into the IGM. Extended gaseous halos around normal star-forming galaxies (excluding galaxies in dense gaseous environments such as clusters) do not automatically prevent outflows from reaching the IGM, although the power requirements are more exacting than for simply blowing gas out of the disk.

5.2.2. Requirements for escape into the IGM

Unambiguous observational proof of ejection of material into the IGM by outflows requires kinematic evidence of outward motion at $v \gtrsim v_{\text{esc}}$ at heights $z \gtrsim 3H_{\text{g}}$ above the midplane of the host galaxy¹¹. This is

¹¹Note that v , and preferably the summed thermal and kinetic energy, must be assessed on a phase-by-phase basis. The cool shell velocity (as used by, for example Ferrara & Tolstoy 2000; Ferrara et al. 2000), or the temperature of the X-ray emitting plasma (e.g. Wang et al. 1995; Martin 1999), are not particularly meaningful tools for assessing whether gas will be retained. The energy per particle in the hot phases is much greater than that of the cool shell material, and it is likely that the kinetic energy of the X-ray-emitting hot gas can exceed its thermal energy several times (Strickland & Stevens 2000).

observationally challenging, especially given that the most interesting, *i.e.* metal-enriched, gas phases are very tenuous, and very hot and highly ionized. Such observations, even of the denser phases, are unlikely to be accomplished for many years. Nevertheless, what the theoretically-and-observationally motivated argument in the preceding section demonstrates is that it is *likely* that starburst galaxies, even ones as massive as $M \sim 10^{11} M_{\odot}$, and possibly some normal spiral galaxies, do eject material into the IGM. This is consistent with the effective yields and metal-loss scenario presented by Garnett (2002) and Tremonti et al. (in preparation). Put another way, we regard escape as an eminently plausible fate for at least some fraction of the material in superwinds, as currently there are no convincing theoretically or observationally-motivated ways to prevent escape.

6. Summary

Making use of the detailed measurements of the diffuse X-ray emitting gas in and around the sample of seven starburst and 3 normal edge-on spiral galaxies presented in Paper I, we have investigated how the properties of this hot gas correlate with the size, mass, star formation rate and star formation intensity in the host galaxies.

We demonstrate that the extra-planar (*i.e.* halo-region) diffuse X-ray emission in this sample of galaxies is ultimately driven by star formation activity within the disk. Accretion of gas from the IGM, or AGN-driven winds (see Paper I), do not appear to be significant in this sample.

Larger galaxies show more radially and vertically extended diffuse X-ray emission, but beyond this correlation we find no evidence that galactic mass plays any part in determining the diffuse hot phase in the disks and halos of these galaxies. The luminosity of the diffuse X-ray emission, both within the disk and halo, is determined primarily by the rate of mechanical energy injection due to SNe in each galaxy (which is correlated to the star-formation rate). The surface brightness of the extra-planar diffuse X-ray emission correlates with the star formation rate per unit area in the underlying disk, but this correlation is a combination of the previously mentioned luminosity and size correlations.

The properties of the diffuse X-ray emission in the normal spiral galaxies is very similar to that found in the starburst superwind galaxies. In fact, one could

successfully predict the diffuse X-ray properties of all three normal galaxies in this sample based on extrapolating the X-ray properties of the starburst galaxies to the lower star formation intensities seen in the normal galaxies. The close similarity in the halo-region diffuse X-ray emission in the starburst (with superwinds) and the normal spirals (presumably with star-formation-fed galactic fountains) is intriguing, and deserves more study. Is it simply due to similar, microphysical, emission mechanisms, or does the similarity extend to the macroscopic hydrodynamics at work over multi-kpc scales?

We also consider what the observed extra-planar diffuse X-ray emission can tell us about the both the efficiency of massive star mechanical feedback on galactic scales, and the accuracy of standard theoretical models of superbubble blow out from disk galaxies.

We find the ratio of the halo-region diffuse X-ray flux to the host galaxy's total FIR flux is typically $f_{X,HALO}/f_{FIR} \sim 4 \times 10^{-5}$, to within a factor two, for both the starburst galaxies and NGC 891. This ratio is independent of the star formation rate per unit area or the mass of the host galaxy.

Assuming that $\sim 1\%$ of the mechanical power flowing into the halo is radiated in the soft X-ray band implies that $\sim 25\%$ of the total mechanical energy released in the disk by SNe is advected into the halo (physically, this is the product of the massive star supernova thermalization efficiency ϵ , and the fraction of the SNe in the star-forming disk able to contribute to driving superbubbles Υ).

We argue that the standard analytical model describing the critical mechanical luminosity for blow-out of superbubble from an exponential disk (originally formulated to Mac Low & McCray 1988) should be reformulated, when considering blow out of gas from the disk on a galactic scale, to allow a significant fraction of all SN energy with a disk area $\sim \pi H_g^2$ to be used (*i.e.* separate star-forming clusters can work together). The standard theoretical formulation, widely applied in theoretical considerations of metal ejection from galaxies (Ferrara & Tolstoy 2000; Ferrara et al. 2000), in which the maximum mechanical energy return is limited by the size of the most massive single OB associations, fails to explain the presence and luminosity of the extra-planar X-ray emission in the halo of the normal spiral NGC 891 (let alone the starbursts!).

We propose that the presence of hot gas in the ha-

los of normal spiral galaxies can be used to directly test the basic theory of superbubble blow out, which predicts the minimum SN rate per unit area required to drive hot gas into the halo. Currently application of this method is limited by the lack of deep X-ray observations of normal spiral galaxies, and uncertainties in the observational determination of SN rate per unit area in even nearby, well-studied galaxies. However, both of these problems should be solved in the next few years by *Chandra*, *XMM-Newton* and *SIRTF* observations.

Finally, we apply this collective-action blow out theory to blow out from the extended gaseous halos of these galaxies. Blow out from the halo into the IGM is energetically more difficult than blow out from the disk into the halo. Nevertheless, it is still probable that the hot, metal-enriched gas in superwinds does escape into the IGM, even for galaxies in normal environments (*i.e.* not in dense galaxies groups or clusters) as massive as $M \sim 10^{10} - 10^{11} M_\odot$. The crucial spatial region around a galaxy that controls whether gas will escape into the IGM is not the outer halo ~ 100 kpc from the host galaxy, but the inner few halo scale heights, within ~ 20 kpc of the galaxy plane.

Within the next few years it will be possible to calibrate theories of disk blow out and mechanical energy feedback against observations of local star-forming galaxies, and thus make meaningful inferences about the enrichment of the IGM by outflows, and the influence of massive star feedback on cosmological scales.

Over the several years this project has been in the making, we have been fortunate to benefit from the insightful comments and questions of many astronomers, too numerous to mention individually, to whom we extend our thanks. We would also like to thank S. Hameed for providing us with R-band and H α images of NGC 1482.

DKS is supported by NASA through *Chandra* Postdoctoral Fellowship Award Number PF0-10012, issued by the *Chandra* X-ray Observatory Center, which is operated by the Smithsonian Astrophysical Observatory for and on behalf of NASA under contract NAS8-39073.

This research is partially based on data from the ING Archive. This publication makes use of data products from the Two Micron All Sky Survey, which is a joint project of the University of Massachusetts and the Infrared Processing and Analysis Center/California

Institute of Technology, funded by the National Aeronautics and Space Administration and the National Science Foundation. Furthermore, this research has made use of the extremely-useful NASA/IPAC Extragalactic Database (NED) which is operated by the Jet Propulsion Laboratory, California Institute of Technology, under contract with the National Aeronautics and Space Administration.

REFERENCES

Aguirre, A., Hernquist, L., Schaye, J., Weinberg, D.H., Katz, N. & Gardner, J., 2001, ApJ, 560, 590

Armus, L., Heckman, T.M., Weaver, K.A. & Lehnert, M.D., 1995, ApJ, 445, 666

de Avillez, M.A., 2000, MNRAS, 315, 479

Murakami, I. & Babul, A., MNRAS, 309, 161

Bell, E.F. & de Jong, R.S., 2001, ApJ, 550, 212

Benson, A.J., Bower, R.G., Frenk, C.S. & White, S.D.M., 2000, MNRAS, 314, 557

Bessel, M.S., Castelli, F. & Plez, B., 1998, A&A, 333, 231

Bottema, R. & Gerritsen, J.P.E., 1997, MNRAS, 290, 585

Brandl, B., Sams, B.J., Bertoldi, F., Eckart, A., Genzel, R., Drapatz, S., Hofmann, R., Löwe, M. & Quirrenbach, A., 1996, ApJ, 466, 254

Bregman, J.N., 1980, ApJ, 236, 577

Bregman, J.N. & Glassgold, A.E., 1982, ApJ, 263, 564

Bregman, J.N. & Houck, J.C., 1997, ApJ, 485, 159

Bregman, J.N. & Pildis, R.A., 1994, ApJ, 420, 570

Burstein, D. & Heiles, C., 1982, AJ, 87, 1165

Carpenter, J.M., 2001, AJ, 121, 2851

Castor, J., McCray, R., Weaver, R., 1975, ApJ, 200, L107

Chandra, R., Leitherer, C., Tremonti, C. & Calzetti, D., 2003, 586, 939

Chevalier, R. & Clegg, A., 1985, Nature, 317, 44

Chiang, W.-H., Ryu, D. & Vishniac, E.T., 1988, PASP, 100, 1386

Chu, Y.-H. & Mac Low, M.-M., 1990, ApJ, 365, 510

Condon, J.J., 1994, ARA&A, 30, 575

Condon, J.J., Cotton, W.D., Greisen, E.W., Yin, Q.F., Perley, R.A., Taylor, G.B., Broderick, J.J., 1998, AJ, 115, 1693

Cox, D.P., ApJ, 245, 534

Cui, W., Sanders, W.T., McCammon, D., Snowden, S.L. & Womble, D.S., 1996, ApJ, 468, 102

Dahlem, M., Golla, G., Whiteoak, J. B., Wielebinski, R., Huettemeister, S. & Henkel, C., 1993, A&A, 270, 29

Dahlem, M., Lazendic, J.S., Haynes, R.F., Ehle, M. & Lisenfeld, U., 2001, A&A, 374, 42

Dahlem, M., Weaver, K.A. & Heckman, T.M. 1998, ApJS, 118, 401

Dale, D.A., et al., 2000, AJ, 120, 583

de Grijjs, R., O'Connell, R.W. & Gallagher, J.S., 2001, AJ, 121, 768

Dekel A., Silk J., 1986, ApJ, 303, 39

Dettmar, R.-J., 1992, Fundamentals of Cosmic Physics, 15, 143

Dettmar, R.-J., 1998, in The Local Bubble and Beyond, D., Breitschwerdt, M.J., Freyberg, & J. Truemper, (Springer-Verlag: Berlin Heidelberg New York), 527

de Vaucouleurs G., de Vaucouleurs A., Corwin Jr. H.G., Buta R.J., Paturel G. & Fouque P., 1991, *Third Reference Catalogue of Bright Galaxies (RC3)* (Springer-Verlag: New York)

De Young, D.S. & Heckman T.M., 1994, ApJ, 431, 598

Douglas, J.N., Bash, F.N., Arakel Bozyan, F., Torrence, G.W., Wolfe, C., 1996, AJ, 111, 1945

Ehle, M., Pietsch, W., Beck, R. & Klein, U., 1998, A&A, 329, 39

Elfhag, T., Booth, R.S., Hoglund, B., Johansson, L.E.B. & Sandqvist, Aa., 1996, A&AS, 115, 439

Elmouttie, M., Haynes, R.F., Jones, K.L., Ehle, M., Beck, R., Harnett, J.I. & Wielebinski, R., 1997, MNRAS, 284, 830

Engelbracht, C.W., Rieke, M. J., Rieke, G.H., Kelly, D.M., Achtermann, J.M., 1998, *ApJ*, 505, 639

Fabbiano, G. 1989, *ARA&A*, 27, 87

Fabbiano, G., Heckman, T.M., Keel, W.C., 1990, *ApJ*, 355, 442

Fabbiano, G. & Juda, J.Z., 1997, *ApJ*, 476, 666

Fabbiano, G. & Shapley, A., 2002, *ApJ*, 565, 908

Fabbiano, G. & Trinchieri, G., 1984, *ApJ*, 286, 491

Ferrara, A., Pettini, M. & Shchekinov, Y., 2000, *MNRAS*, 319, 539

Ferrara, A. & Tolstoy, E., 2000, *MNRAS*, 313, 291

Figer, D.F., et al., 2002, *ApJ*, 581, 258

Förster Schreiber, N.M., Genzel, R., Lutz, D., Kunze, D. & Sternberg, A., 2001, *ApJ*, 552, 544

Freedman, W.L., et al., 1994, *ApJ*, 427, 628

Garnett, D.R., 2002, *ApJ*, 581, 1019

Golla, G., 1999, *A&A*, 345, 778

Golla, G. & Wielebinski, R., 1994, *A&A*, 286, 733

Hameed, S. & Devereux, N., 1999, *AJ*, 118, 730

Heckman, T.M., 1999, *Ap&SS*, 266, 3

Heckman, T. M., Armus, L., & Miley, G. K. 1990, *ApJS*, 74, 833

Heckman, T.M., Sembach, K.R., Meurer, G.R., Strickland, D.K., Martin, C.L., Calzetti, D. & Leitherer, C., 2001, *ApJ*, 554, 1021

Hillenbrand, L.A. & Hartmann, L.W., 1998, *ApJ*, 492, 540

Hollenbach, D.J. & Tielens, A.G.G.M., 1997, *ARA&A*, 35, 179

Hoopes, C.G., Heckman, T.M., Strickland, D.K. & Howk, J.C., 2003, submitted for publication in *ApJ*

Hoopes, C.G., Walterbos, R.A.M. & Rand, R.J., 1999, *ApJ*, 552, 669

Howk, J.C. & Savage, B.D., 1999, *AJ*, 117, 2077

Ichikawa, T., Yanagisawa, K., Itoh, N., Tarusawa, K., van Driel, W. & Ueno, M., 1995, *AJ*, 109, 2038

Irwin, J.S. & Seaquist, E.R., 1991, *ApJ*, 371, 111

Irwin, J.S. & Sofue, Y., 1996, *ApJ*, 464, 738

Jaaret, T.H., Chester, T., Cutri, R., Schneider, S. & Huchra, J.P., 2003, *AJ*, 125, 525

Karachentsev I.D. & Sharina M.E., 1997, *A&A*, 324, 457

Katz, N., Keres, D., Davé, R. & Weinberg, D.A., 2002, in *The IGM/Galaxy Connection- The Distribution of Baryons at z=0*, astro-ph/0209279

Kennicutt, R.C., 1998a, *ApJ*, 498, 541

Kennicutt, R.C., 1998b, *ARA&A*, 36, 189

Koo, B.-C. & McKee, C.F., 1992, *ApJ*, 388, 93

Koornneef, J., 1993, *ApJ*, 403, 581

Kruit, P.C. van der, 1984, *A&A*, 140, 470

Kruit, P.C. van der, & de Grijs, R., 1999, *A&A*, 352, 129

Kuntz, K.D. & Snowden, S.L., 2000, *ApJ*, 543, 195

Larson, R.B., 1974, *MNRAS*, 169, 229

Lehnert, M. & Heckman, T.M., 1995, *ApJS*, 97, 89

Lehnert, M. & Heckman, T.M., 1996, *ApJ*, 472, 546

Lira, P., Johnson, R. & Lawrence, A., 2002, *MNRAS* in press (astro-ph/0206123)

Lynds, C.R. & Sandage, A.R., 1963, *ApJ*, 137, 1005

McCarthy, P.J., Heckman, T.M. & van Breugel, W. 1987, *AJ*, 92, 264

McKee, C.F., 1995, in *ASP Conf Series* 80, *The Physics of the Interstellar Medium*, A. Ferrara, C.F. McKee, C. Heiles & P.R. Shapiro (San Francisco: ASP), 292

McKee, C.F. & Ostriker, J.P., 1977, *ApJ*, 218, 148

McKeith, C.D., Greve, A., Downes, D. & Prada, F., 1995, *A&A*, 293, 703

McLeod, K.K., Rieke, G.H., Rieke, M.J. & Kelly, D.M., 1993, *ApJ*, 412, 111

Mac Low, M.-M., 1996, in “The Interplay between Massive Star Formation, the ISM, and Galaxy Evolution,” eds. D. Kunth et al., (Paris: Editions Frontières), 169

Mac Low, M.-M. & Ferrara, A., 1999, ApJ, 513, 142

Mac Low, M.-M. & McCray, R., 1988, ApJ, 324, 776

Mac Low, M.-M., McCray, R., & Norman, M.L., 1989, ApJ, 337, 141

Malumuth, E.M. & Heap, S.R., 1994, AJ, 107, 1054

Martin, C.L., 1999, ApJ, 513, 156

Martin, C.L., 1996, ApJ, 465, 680

Meurer, G.R., Heckman, T.M., Leitherer, C., Kinney, A., Robert, C & Garnett, D.R., 1995, AJ, 110, 2665

Mewe R., Kaastra J. S., Liedahl D. A., 1995, Legacy, 6, 16

Nordgren, T.E., Cordes, J.M. & Terzian, Y., 1992, AJ, 104, 1465

Norman, C.A. & Ferrara, A., 1996, ApJ, 467, 280

Norman, C. A. & Ikeuchi, S., 1989, ApJ, 345, 372

O’Connell, R.W., Gallagher, J.S., Hunter, D.A. & Colley, W.N., 1995, ApJ, 446, L1

Olling, R.P., 1996, AJ, 112, 457

Ott, M., Whiteoak, J.B., Henkel, K. & Wielebinski, R., 2001, A&A, 372, 463

Pence, W.D., 1981, ApJ, 247, 473

Press, W.H., Teukolsky, S.A., Vetterling, W.T. & Flannery, B.P., 1992, in Numerical Recipes in FORTRAN: The Art of Scientific Computing – Second Edition (New York: Cambridge University Press), 637

Puche, D., Carignan, C., 1988, AJ, 95, 1025

Puche, D., Carignan, C., van Gorkom, J.H., 1991, AJ, 101, 456

Pudritz, R.E. & Fiege, J.D., 2000, in ASP Conf. Series 168, New Perspectives on the Interstellar Medium, A.R. Taylor, T.L. Landecker & G. Joncas, (San Francisco: ASP), 235

Rand, R., 1994, A&A, 285, 833

Rand, R.J., 1996, ApJ, 462, 712

Rand, R.J., Kulkarni, S.R. & Hester, J.J., 1990, ApJ, 352, 1

Read, A.M., 1994, Ph.D. Thesis (University of Birmingham, UK)

Read, A.M. & Ponman, T.J., 2001, MNRAS, 328, 127

Read, A.M., Ponman, T.J., Strickland, D.K., 1997, MNRAS, 286, 626

Reynolds, R.J., 1989, ApJ, 339, L29

Rice, W., Lonsdale, C.J., Soifer, B.T., Neugebauer, G., Kopan, E.L., Llyod, L.A., deJong, T. & Habing, H.J., 1988, ApJS, 68, 91

Rieke, G.H., Loken, K., Rieke, M.J. & Tamblyn, P., 1993, ApJ, 412, 99

Rossa, J. & Dettmar, R.-J., 2003, A&A, in press

Rossa, J. & Dettmar, R.-J., 2000, A&A, 359, 433

Roth, J., Mould, J.R. & Davies, R.D., 1991, AJ, 102, 1303

Rupen, M.P., 1991, AJ, 102, 48

Sanders, D.B. & Mirabel, I.F., 1996, ARA&A, 34, 749

Satyapal, S., Watson, D.M., Pipher, J.L., Forrest, W.J., Greenhouse, M.A., Smith, H.A., Fischer, J. & Woodward, C.E., 1997, ApJ, 483, 148

Sembach, K.R. & Danks, A.C., 1994, A&A, 289, 539

Shapiro, P.R. & Field, G.B., 1976, ApJ, 205, 762

Shapiro, P.R., Giroux, M.L. & Babul, A., 1994, ApJ, 427, 25

Shapley, A., Fabbiano, G. & Eskridge, P., 2001, ApJS, 137, 139

Shopbell, P.L., Bland-Hawthorn, J., 1998, ApJ, 493, 129

Shull, J.M. & Slavin, J.D., 1994, ApJ, 427, 784

Silich, S.A. & Tenorio-Tagle, G., 1998, MNRAS, 299, 249

Silich, S.A. & Tenorio-Tagle, G., 2001, ApJ, 552, 91

Snowden, S.L. & Pietsch, W., 1995, ApJ, 452, 627

Sofue, Y., Wakamatsu, K. & Malin, D.F., 1994, AJ, 108, 2102

Sofue, Y., 1997, PASJ, 49, 17

Soifer, B.T., et al., 1989, AJ, 98, 1766

Soifer, B.T., Sanders, D.B., Madore, B.F., Neugebauer, G., Danielson, G.E., Elias, J.H., Lonsdale, C.J. & Rice, W.L., 1987, ApJ, 320, 238

Sommer-Larsen, J., Toft, S., Rasmussen, J., Pedersen, K., Gotz, M. & Portinari, L., 2002, to appear in "The Evolution of Galaxies. III. From simple approaches to self-consistent models," Eds. G. Hensler et al., (astro-ph/0210514)

Sorai, K., Nakai, N., Kuno, N., Nishiyama, K. & Hasegawa, T., 2000, PASJ, 52, 785

Strickland, D.K., Heckman, T.M., Weaver, K.A. & Dahlem, M., 2000, AJ, 120, 2965

Strickland, D.K., Ponman, T.J. & Stevens, I.R., 1997, A&A, 320, 378

Strickland, D.K. & Stevens, I.R., 1999, MNRAS, 306, 43

Strickland, D.K. & Stevens, I.R., 2000, MNRAS, 314, 511

Strickland, D.K., Heckman, T.M., Colbert, E.J.M., Hoopes, C.G. & Weaver, K.A., 2002b, to appear in the proceedings of IAU 212 "A Massive Star Odyssey, from Main Sequence to Supernova," Eds. K.A. van der Hucht, A. Herrero & C. Esteban (astro-ph/0207177)

Strickland, D.K., Heckman, T.M., Colbert, E.J.M., Hoopes, C.G. & Weaver, K.A., 2003, submitted to ApJS (Paper I)

Strickland, D.K., Heckman, T.M., Weaver, K.A., Hoopes, C.G. & Dahlem, M., 2002a, ApJ, 568, 689

Suchkov, A.A., Balsara, D.S., Heckman, T.M., Leitherer, C., 1994, ApJ, 430, 511

Tenorio-Tagle, G., 1996, AJ, 111, 1641

Thornton, K., Gaudlitz, M., Janka, H.-Th. & Steinmetz, M., 1998, ApJ, 500, 95

Toft, S., Rasmussen, J., Sommer-Larsen, J. & Pedersen, K., 2002, MNRAS, 335, 799

Tremonti, C., Calzetti, D., Leitherer, C. & Heckman, T.M., 2001, ApJ, 555, 322

Tremonti, C.A., et al., in preparation

Tully, R.B. & Fouqué, P., 1985, ApJS, 58, 67

Vogler, A., Pietsch, W. & Kahabka, P., 1995, A&A, 305, 71

Voit, G.M., 1996, ApJ, 465, 548

Wainscoat, R.J., de Jong, T. & Wesselius, P.R., 1987, A&A, 181, 225

Wang, Q.D., Immler, S., Walterbos, R., Lauroesch, J.T. & Breitschwerdt, D., 2001, ApJ, 555, L99

Wang, Q.D., Walterbos, R.A.M., Steakley, M.F., Norman, C.A. & Braun, R., 1995, ApJ, 439, 176

Weaver R., McCray R., Castor J., Shapiro P., Moore R., 1977, ApJ, 218, 377

Weliachew, I., Fomalont, E.B. & Greisen, E.W., 1984, A&A, 137, 335

Wiseman, J.J. & Ho, P.T.P., 1998, ApJ, 502, 676